UNIVERSIDAD DE CONCEPCIÓN

Centro de Investigación en Ingeniería Matemática (CI^{2}MA)

A diffusively corrected multiclass Lighthill-Whitham-Richards traffic model with anticipation lengths and reaction times

Raimund Bürger, Pep Mulet,
Luis M. Villada

PREPRINT 2012-25

SERIE DE PRE-PUBLICACIONES

A DIFFUSIVELY CORRECTED MULTICLASS LIGHTHILL-WHITHAM-RICHARDS TRAFFIC MODEL WITH ANTICIPATION LENGTHS AND REACTION TIMES

RAIMUND BÜRGER[A], PEP MULET[B], AND LUIS M. VILLADA[C]

Abstract. Multiclass Lighthill-Whitham-Richards traffic models [Benzoni-Gavage and Colombo, *Eur. J. Appl. Math.* 14:587–612 (2003); Wong and Wong, *Transp. Res. A* 36:827–841 (2002)] give rise to first-order systems of conservation laws that are hyperbolic under usual conditions, so that their associated Cauchy problems are well-posed. Anticipation lengths and reaction times can be incorporated into these models by adding certain conservative second-order terms to these first-order conservation laws. These terms can be diffusive under certain circumstances, thus, in principle, ensuring the stability of the solutions. The purpose of this paper is to analyze the stability of these diffusively corrected models under varying reaction times and anticipation lengths. It is demonstrated that instabilities may develop for high reaction times and short anticipation lengths, and that these instabilities may have controlled frequencies and amplitudes due to their nonlinear nature.

1. Introduction

1.1. **Scope.** The well-known Lighthill-Whitham-Richards (LWR) kinematic traffic model [20, 28] states that the density of cars $\phi = \rho/\rho_{\max}$, where ρ is the local number of cars per mile and $\rho_{\max}$ is some maximum bumper-to-bumper density, can be described by the conservation law $\partial_t \phi + \partial_x(\phi v(\phi))_x = 0$, where t is time, x is the spatial coordinate along either an unbounded, one-directional highway or a closed circuit, and the local velocity $v = v(x,t)$ is a given function of the local density, $v = v(\phi(x,t))$. It is usually assumed that $v(\phi) = v^{\max} V(\phi)$, where $v^{\max}$ is the preferential velocity of drivers on a free highway and V is a hindrance function describing the drivers' behaviour of reducing speed in presence of other cars. The function V satisfies $V(0) = 1$ and $V'(\phi) \le 0$. These assumptions lead to the one-dimensional scalar conservation law

$$\partial_t \phi + \partial_x f(\phi) = 0, \quad x \in \mathbb{R}, \quad t > 0, \tag{1.1}$$

were the flux density function f is given by

$$f(\phi) = \phi v(\phi) = v^{\max} \phi V(\phi). \tag{1.2}$$

Date: November 8, 2012.

[A]CI^{2}MA and Departamento de Ingeniería Matemática, Facultad de Ciencias Físicas y Matemáticas, Universidad de Concepción, Casilla 160-C, Concepción, Chile. E-Mail: rburger@ing-mat.udec.cl.

[B]Departament de Matemàtica Aplicada, Universitat de València, Av. Dr. Moliner 50, E-46100 Burjassot, Spain. E-Mail: mulet@uv.es.

[C]CI^{2}MA and Departamento de Ingeniería Matemática, Facultad de Ciencias Físicas y Matemáticas, Universidad de Concepción, Casilla 160-C, Concepción, Chile. E-Mail: lmvillada@ing-mat.udec.cl.

The model (1.1), (1.2) has been extended in several directions. On one hand, Nelson [22, 23] showed that introducing an anticipation length L and a reaction time τ, replacing $V(\phi(x,t))$ by $V(\phi(x+L-v^{\max}V\tau,t-\tau))$ and neglecting $\mathcal{O}(L^2+\tau^2)$ terms when expanding the latter expression around (x,t), one obtains a "diffusively corrected" version of (1.1), (1.2) of the following form:

$$\partial_t\phi + \partial_x f(\phi) = A(\phi)_{xx}. \tag{1.3}$$

Here, L may also depend on ϕ, and under certain restrictions on $L = L(\phi)$, τ and $v(\phi)$, the funcion A is Lipschitz continuous and increasing so that the governing equation (1.3) of the diffusively corrected LWR model ("DCLWR model") is a strongly degenerate parabolic PDE in the sense that $A(\phi) = 0$ for $\phi \le \phi_c$, where ϕ_c is a critical density value (e.g., a perception threshold), and $A'(\phi) > 0$ for $\phi > \phi_c$. Properties of (1.3), under the additional assumption of abruptly varying road surface conditions, were analyzed in [8]. On the other hand, Benzoni-Gavage and Colombo [3] and Wong and Wong [33] extended the LWR model (1.1), (1.2) to a multi-class model, the so-called "MCLWR model", by distinguishing N classes of drivers associated with preferential velocities $v_1^{\max} > v_2^{\max} > \cdots > v_N^{\max}$. For the MCLWR model, the sought quantity is the vector $\Phi := (\phi_1,\dots,\phi_N)^{\mathrm{T}}$ of the densities ϕ_i of the cars of the different driver classes. The local velocity v_i of vehicles of driver class i is given by $v_i = v_i(\phi) = v_i^{\max}V(\phi)$ for $i = 1,\dots,N$, where we define $\phi := \phi_1+\cdots+\phi_N$. Thus, the MCLWR model is given by a strongly coupled system of nonlinear first-order conservation laws of the type

$$\partial_t\Phi + \partial_x\boldsymbol{f}(\Phi) = \boldsymbol{0}, \quad x\in\mathbb{R}, \quad t>0; \quad \boldsymbol{f}(\Phi) = \big(f_1(\Phi),\dots,f_N(\Phi)\big)^{\mathrm{T}}, \tag{1.4}$$

where the components of the flux vector $\boldsymbol{f}(\Phi)$ are given by

$$f_i(\Phi) = \phi_i v_i(\phi) = \phi_i v_i^{\max}V(\phi), \quad i = 1,\dots,N. \tag{1.5}$$

It can be shown [14, 35] that the system (1.4), (1.5) is strictly hyperbolic for $\Phi \in \mathcal{D}^0 := \{\Phi\in\mathbb{R}^N \mid \phi_1>0,\dots,\phi_N>0,\phi<1\}$.

It is the purpose of this paper to introduce a new model, called diffusively corrected multi-class LWR model ("DCMCLWR model"), by combining the assumptions of the DCLWR model with those of the MCLWR model. In particular, we associate class i of drivers with the triple $(v_i^{\max},L_i,\tau_i)$, $i=1,\dots,N$, which means that drivers of different classes may have different preferential velocities, anticipation lengths, and reaction times. The resulting model, which reduces to (1.3) and (1.4) in the respective limit cases $N=1$ and $\boldsymbol{L}=\boldsymbol{0}$, $\boldsymbol{\tau}=\boldsymbol{0}$, where $\boldsymbol{L} := (L_1,\dots,L_N)^{\mathrm{T}}$ and $\boldsymbol{\tau} := (\tau_1,\dots,\tau_N)^{\mathrm{T}}$, can be cast as a quasi-linear system of second-order PDEs of the form

$$\partial_t\Phi + \partial_x\boldsymbol{f}(\Phi) = \partial_x\big(\boldsymbol{B}(\Phi)\partial_x\Phi\big). \tag{1.6}$$

Here the flux vector $\boldsymbol{f} = \boldsymbol{f}(\Phi)$ is the same as in the MCLWR model, and $\boldsymbol{B} = \boldsymbol{B}(\Phi)$ is an $N\times N$ matrix expressing the diffusive correction. The precise functional form of $\boldsymbol{B}(\Phi)$ depends on the choice of $V(\phi)$ and the vectors of parameters $\boldsymbol{v}^{\max} := (v_1^{\max},\dots,v_N^{\max})^{\mathrm{T}}$, $\boldsymbol{L}$ and $\boldsymbol{\tau}$.

The system (1.6) is supplied with an initial condition and periodic boundary conditions. We formulate, and in part evaluate, a stability criterion for the model (1.6) based on an analysis of the eigenvalues of the matrices

$$\boldsymbol{M}(\Phi,\xi) := \frac{\mathrm{i}}{\xi}\mathcal{J}_{\boldsymbol{f}}(\Phi) + \boldsymbol{B}(\Phi) \in \mathbb{C}^{N\times N}, \quad \xi\in\mathbb{R}_+, \tag{1.7}$$

where $\mathrm{i} = \sqrt{-1}$ and $\mathcal{J}_{\boldsymbol{f}}(\Phi)$ denotes the Jacobian matrix of $\boldsymbol{f}(\Phi)$. Furthermore, by a series of numerical experiments we illustrate the behaviour of solutions to (1.6), and in particular the effect of different values of L_i and τ_i for different classes of drivers.

1.2. **Related work.** To put the paper into the proper perspective, we mention first that the MCLWR model has been analyzed in a number of papers including [4, 15, 21, 35]. In particular, its hyperbolicity has been established [15, 35] and the admissible waves of the Riemann problem have been investigated [35]. Moreover, the model (1.4), (1.5) admits a separable, strictly convex entropy since the corresponding Jacobian matrix $\mathcal{J}_{\boldsymbol{f}}(\Phi)$ is diagonally symmetrizable [3, 4]. Componentwise or characteristic high-resolution numerical schemes for (1.4), (1.5) involving weighted essentially non-oscillatory (WENO) flux reconstructions are advanced in [11, 14, 34, 36]. On the other hand, particularly simple first- and second-order difference schemes for the same problem that rely on the structure of the fluxes f_i (1.5) along with the definite sign of the velocities v_i are introduced in [7]. Variants of the original MCLWR model (in the sense of [3, 33]) have been proposed and in part analyzed for highways with varying road surface conditions [10, 37, 38], traffic flow on networks [17, 24], and stochastic fundamental diagrams (equivalent to the velocity functions v_i) [25].

Several alternative approaches have been pursued to extend the LWR model to finite reaction times and anticipation lengths. The treatment by Sopasakis and Katsoulakis [31] (see also [18]) for one driver class leads to a scalar conservation law with a non-local flux involving a non-symmetric "anticipation kernel". In [26] a linear stability analysis is applied to a second-order macroscopic local traffic model, and a corrected "effective density" sensor accounts for aggressive or timid drivers. A related analysis is presented in [30]. Ngoduy and Tampere [27] study the influence of different reaction times (of a single driver class) in terms of the same model. Their condition for traffic stability reads [27, Eq. (39)]

$$\tau < \frac{1}{2\phi^2 |V'(\phi)| v^{\max}} \quad \text{for } 0 < \phi < 1 \tag{1.8}$$

(in our notation). If this condition is violated, then their model can develop instabilities that can be considered as stop-and-go waves. The relation between reaction times and anticipation lengths and traffic stability is also discussed in [32].

Finally, we mention that other kinematic flow models that give rise to systems of the type (1.6) include the sedimentation of polydisperse suspensions [5] and the settling and creaming of dispersions of droplets [1]. These models are typically posed with zero-flux boundary conditions on a bounded x-interval.

1.3. **Outline of the paper.** The remainder of this paper is organized as follows. In Section 2 we describe the DCMCLWR model accounting for anticipation lengths and reaction times. In Section 3 a parabolicity analysis is performed and its results are confirmed by the numerical experiments described in Section 4. Some conclusions are drawn in Section 5.

2. A diffusively corrected MCLWR model

2.1. **The model equations.** Assume that vehicles of class i have the preferential velocity $v_i^{\max}$, where

$$v_1^{\max} \geq v_2^{\max} \geq \cdots \geq v_N^{\max} > 0. \tag{2.1}$$

Following the reasoning in [22] (see also [8]), we now assume that the behavior of drivers of class i is associated with an anticipation distance L_i and a reaction time τ_i. Then the reaction of the driver does not depend on the spot value $\phi(x,t)$, but rather on

$$p_i(x,t) := \phi\left(x + L_i - v_i^{\max} V \tau_i, t - \tau_i\right). \tag{2.2}$$

This formulation takes into account that $v_i^{\max} V \tau_i$ is the distance travelled by a car of class i in a time interval of length τ_i. Furthermore, note that (as in [8]) notation is ambiguous in (2.2) since we are not specific about the argument of V inside (2.2). To turn (2.2) into a usable expression for the flux f_i, we expand $V(p_i(x,t))$ around $\phi(x,t)$. Writing $\phi = \phi(x,t)$ and denoting

$$\tau := \max_{1\leq i\leq N} \tau_i, \quad L := \max_{1\leq i\leq N} L_i,$$

we obtain

$$V(p_i(x,t)) = V(\phi) + V'(\phi)\Big(\partial_x\phi\big(L_i - v_i^{\max}V(\phi)\tau_i\big) - \tau_i\partial_t\phi\Big) + \mathcal{O}(\tau^2 + L^2). \tag{2.3}$$

Summing the conservation laws $\partial_t\phi_i + \partial_x(v_i^{\max}\phi_i V(\phi)) = 0$ over $i = 1,\ldots,N$ and defining $\boldsymbol{v}^{\max} := (v_1^{\max},\ldots,v_N^{\max})^{\mathrm{T}}$ yields

$$\partial_t\phi = \sum_{k=1}^{N} \partial_t\phi_k = -\partial_x\big(V(\phi)\Phi^{\mathrm{T}}\boldsymbol{v}^{\max}\big).$$

Inserting this result into (2.3) we get

$$\begin{aligned} V(p_i(x,t)) = V(\phi) + V'(\phi)\Big(\big(L_i - \tau_i v_i^{\max}V(\phi)\big)\partial_x\phi + \tau_i\partial_x\big(V(\phi)\Phi^{\mathrm{T}}\boldsymbol{v}^{\max}\big)\Big) \\ + \mathcal{O}(\tau^2 + L^2). \end{aligned}$$

Neglecting the $\mathcal{O}(\tau^2 + L^2)$ term and inserting the remaining expression into the conservation equations

$$\partial_t\phi_i(x,t) + \partial_x\big(\phi_i(x,t)v_i(x,t)\big) = 0, \quad v_i(x,t) = v_i^{\max}V\big(p_i(x,t)\big), \quad i = 1,\ldots,N,$$

we obtain a system of the form (1.6), where the components of the flux vector $\boldsymbol{f}(\Phi)$ are given by (1.5) and, if we assume for a moment that no perception threshold for the anticipation length or reaction time is introduced, then the entries of the diffusion matrix $\boldsymbol{B}(\Phi)$ are given by

$$\begin{aligned} \alpha_{ij}(\Phi) = -V'(\phi)\left(L_i + \tau_i\left[V'(\phi)\Phi^{\mathrm{T}}\boldsymbol{v}^{\max} + (v_j^{\max} - v_i^{\max})V(\phi)\right]\right)\phi_i v_i^{\max}, \\ 1 \leq i,j \leq N. \end{aligned} \tag{2.4}$$

We recall that the entries of $\mathcal{J}_{\boldsymbol{f}}(\Phi) = (\partial f_i(\Phi)/\partial\phi_j)_{i,j=1,\ldots,N}$ are given by

$$\frac{\partial f_i(\Phi)}{\partial\phi_j} = v_i^{\max}\big(\delta_{ij}V(\phi) + \phi_i V'(\phi)\big), \quad i,j = 1,\ldots,N.$$

In this paper we focus on the hindrance functions V according to Dick [13] and Greenberg [16], namely

$$V(\phi) = \min\{1, -C\ln\phi\} = \begin{cases} 1 & \text{for } \phi \le \phi_{\mathrm{DG}}, \\ -C\ln\phi & \text{for } \phi > \phi_{\mathrm{DG}} \end{cases} \tag{2.5}$$

with a parameter $C > 0$, where we employ the common value $C = \mathrm{e}/7 \approx 0.38833$ such that $\phi_{\mathrm{DG}} = \exp(-1/C) \approx 0.076142$. Alternatively we use the common linear Greenshields (GS) velocity function

$$V(\phi) = 1 - \phi. \tag{2.6}$$

Note that in view of (2.4), the particular form of the velocity function (2.5) implies that $B(\Phi) = 0$ for $\phi \le \phi_{\mathrm{c}} = \phi_{\mathrm{DG}}$, so (1.6) degenerates to the first-order system (1.4) for the corresponding vectors Φ. Thus, the resulting model is strongly degenerate. In general, and following [29], we assume that ϕ_{c} is an explicitly known perception threshold or critical density such that the drivers' reaction is instantaneous in relatively free flow, i.e. when $\phi \le \phi_{\mathrm{c}}$, and otherwise is modeled by the diffusion term. Thus, for a unified treatment we assume that

$$\boldsymbol{B}(\Phi) = \big(B_{ij}(\Phi)\big)_{i,j=1,\dots,N}, \quad \text{where} \quad B_{ij}(\Phi) = \begin{cases} 0 & \text{if } \phi \le \phi_{\mathrm{c}}, \\ \alpha_{ij}(\Phi) & \text{if } \phi > \phi_{\mathrm{c}}. \end{cases} \tag{2.7}$$

2.2. **Stability analysis.** We perform a linearized stability analysis for the system (1.6) under the assumptions of the DCMCLWR model. The linearized equation for a small perturbation $\boldsymbol{u}$ about a constant state $\Phi^{(0)}$ is obtained by substituting $\Phi = \Phi^{(0)} + \boldsymbol{u}$ into (1.6) and neglecting quadratic terms in $\boldsymbol{u}$. This yields the following linearized version of (1.6):

$$\partial_t \boldsymbol{u} + \boldsymbol{J}\partial_x \boldsymbol{u} = \boldsymbol{B}\partial_x^2 \boldsymbol{u}, \quad \text{where } \boldsymbol{J} := \mathcal{J}_{\boldsymbol{f}}\big(\Phi^{(0)}\big),\ \boldsymbol{B} := \boldsymbol{B}\big(\Phi^{(0)}\big). \tag{2.8}$$

We now seek solutions of (2.8) of the form $\boldsymbol{u}(x,t) = \boldsymbol{z}(t;\xi)\exp(\mathrm{i}\xi x)$ for a fixed frequency ξ. The vector function $\boldsymbol{z}$ satisfies the system of ordinary differential equations

$$\boldsymbol{z}' = -\xi^2 \boldsymbol{M}\boldsymbol{z}, \tag{2.9}$$

where $' \equiv \mathrm{d}/\mathrm{d}t$ and $\boldsymbol{M} = \boldsymbol{M}(\Phi^{(0)}, \xi)$ is the matrix defined in (1.7). The general solution of (2.9) is of the well-known form

$$\boldsymbol{z}(t;\xi) = \sum_{j=1}^{r} \exp\big(-\xi^2 \lambda_j t\big)\boldsymbol{q}_j(t,\xi), \tag{2.10}$$

where $\lambda_1, \dots, \lambda_r$ are the eigenvalues of $\boldsymbol{M}$ that appear in its associated Jordan blocks of corresponding sizes $m_1, \dots, m_r$, where $m_1 + \cdots + m_r = N$, and $\boldsymbol{q}_j$ are polynomials (with vectorial coefficients related to the Jordan decomposition basis) of degree less or equal $m_j - 1$. If $\lim_{t\to+\infty} |z(t;\xi)| < \infty$, then $\mathrm{Re}(\lambda_j) \ge 0$ if $m_j = 1$ or $\mathrm{Re}(\lambda_j) > 0$ if $m_j > 1$.

With respect to the instability phenomena predicted by eigenvalue analysis of $\boldsymbol{J}$ and $\boldsymbol{B}$, we mention first that if $\boldsymbol{B}$ has an eigenvalue λ with $\mathrm{Re}(\lambda) < 0$, then it turns out that $\boldsymbol{M}$ will do so for $|\xi| > \xi_0$, for some ξ_0. It would then follow that this would trigger a growth of $\boldsymbol{z}(t;\xi)$ in (2.10) when $t \to \infty$ for $|\xi| > \xi_0$. This would completely ruin the solution of the nonlinear system, for, although the nonlinearity would prevent the amplitude of the oscillations from growing indefinitely, these

oscillations would appear in all frequencies above ξ_0. Milder instabilities would be expected if $\boldsymbol{B}$ has eigenvalues with positive real parts but $\boldsymbol{M}$ does not, since this should only hold for relatively small values of ξ. These phenomena are illustrated in the numerical examples.

Considering separately the two terms of the matrix $\boldsymbol{M}$ (cf. (1.7)), namely $(\mathrm{i}/\xi)\boldsymbol{J}$ and $\boldsymbol{B}$, we obtain that the linearized stability condition for (1.6) when $\boldsymbol{B} = 0$ is exactly the hyperbolicity condition for the resulting system (ξ can take any sign), whereas the linearized stability condition when $\boldsymbol{f} = \boldsymbol{0}$ is directly inherited by the condition on $\boldsymbol{M}$, i.e., the eigenvalues of $\boldsymbol{B} = \boldsymbol{B}(\Phi^{(0)})$ should have non-negative real parts if they are simple and strictly positive real parts if they have some corresponding Jordan block of non-trivial dimension. Unfortunately, $\boldsymbol{J}$ having real eigenvalues and $\boldsymbol{B}$ having eigenvalues with strictly positive real parts does not imply that eigenvalues of $\boldsymbol{M}$ have strictly positive real parts, as the following simple counterexample shows: with $\xi = 1$ and

$$\boldsymbol{J} = \begin{bmatrix} 1 & 0 \\ 0 & -3 \end{bmatrix}, \quad \boldsymbol{B} = \begin{bmatrix} -1 & -3 \\ 3 & 3 \end{bmatrix},$$

the eigenvalues of $\boldsymbol{M} = \mathrm{i}\boldsymbol{J} + \boldsymbol{B}$ are $-0.2332 - 2.2436\mathrm{i}$ and $2.2332 + 4.2436\mathrm{i}$, whereas the eigenvalues of $\boldsymbol{B}$ are $1 \pm 2.2361\mathrm{i}$.

This discussion illustrates that the satisfaction of the stability criterion stipulated by (2.10), namely that the pairwise distinct eigenvalues $\lambda_1, \ldots, \lambda_r$ of the matrix $\boldsymbol{M} = \boldsymbol{M}(\Phi^{(0)}, \xi)$ satisfy

$$\operatorname{Re}\lambda_1 \leq 0, \ldots, \operatorname{Re}\lambda_r \leq 0, \tag{2.11}$$

can in general not be evaluated exactly by analyzing $\boldsymbol{J}$ and $\boldsymbol{B}$ separately. However, some special cases are tractable. These include the DCMCLWR with drivers having the same maximum speed so that classes of drivers are distinguished by their reaction times and anticipation lengths (see Sect. 2.3).

2.3. **DCLWR model with drivers having the same maximum speed.** Let us consider the model (1.5), (1.6), (2.4) under the assumption

$$v_1^{\max} = \cdots = v_N^{\max} =: v^{\max}. \tag{2.12}$$

This means that the classes of vehicles are distinguished only by the drivers' reaction times τ_i and anticipation lengths L_i. Under the assumption (2.12), and defining $\boldsymbol{e} := (1, \ldots, 1)^{\mathrm{T}}$, $\boldsymbol{D_\tau} := \operatorname{diag}(\tau_1, \ldots, \tau_N)$ and $\boldsymbol{D_L} := \operatorname{diag}(L_1, \ldots, L_N)$, we obtain

$$\begin{aligned} \mathcal{J}_{\boldsymbol{f}}(\Phi) &= v^{\max}\big(V(\phi)\boldsymbol{I} + V'(\phi)\Phi\boldsymbol{e}^{\mathrm{T}}\big), \\ \boldsymbol{B}(\Phi) &= -V'(\phi)v^{\max}\big(v^{\max}\phi V'(\phi)\boldsymbol{D_\tau}\Phi + \boldsymbol{D_L}\Phi\big)\boldsymbol{e}^{\mathrm{T}}. \end{aligned} \tag{2.13}$$

Under the present assumptions, and setting $\Phi := \Phi^{(0)}$ and $\phi := \phi^{(0)}$, we obtain

$$\boldsymbol{M} = v^{\max}\left[\frac{\mathrm{i}}{\xi}V(\phi)\boldsymbol{I} + V'(\phi)\left(\frac{\mathrm{i}}{\xi}\Phi - \big(v^{\max}\phi V'(\phi)\boldsymbol{D_\tau} + \boldsymbol{D_L}\big)\Phi\right)\boldsymbol{e}^{\mathrm{T}}\right].$$

This matrix is a rank-one perturbation of a multiple of the identity matrix $\boldsymbol{I}$, and its eigenvalues are given by

$$\begin{aligned} \tilde{\lambda}_1 &= v^{\max}\left[\frac{\mathrm{i}}{\xi}V(\phi) + V'(\phi)\left(\frac{\mathrm{i}}{\xi}\phi - \big(v^{\max}\phi V'(\phi)\boldsymbol{\tau}^{\mathrm{T}} + \boldsymbol{L}^{\mathrm{T}}\big)\Phi\big)\right)\right], \\ \tilde{\lambda}_2 &= \cdots = \tilde{\lambda}_N = v^{\max}\frac{\mathrm{i}}{\xi}V(\phi), \end{aligned} \tag{2.14}$$

with the corresponding one- and $(N-1)$-dimensional eigenspaces

$$\mathcal{V}_1 = \left\{ \boldsymbol{w} \in \mathbb{C}^N \,:\, \boldsymbol{w} = \alpha \left(\frac{\mathrm{i}}{\xi}\Phi - \big(v^{\max}\phi V'(\phi)\boldsymbol{D_\tau} + \boldsymbol{D_L}\big)\Phi \right),\ \alpha \in \mathbb{R} \right\},$$
$$\mathcal{V}_{2,\dots,N} = \big\{ \boldsymbol{w} \in \mathbb{R}^N \,:\, \boldsymbol{e}^{\mathrm{T}}\boldsymbol{w} = 0 \big\},$$

so that all Jordan blocks are trivial. On the other hand, the rank-1 matrix $\boldsymbol{B}(\Phi)$ defined by (2.13) has the eigenvalues

$$\beta_1 = -V'(\phi)v^{\max}\big(v^{\max}\phi V'(\phi)\boldsymbol{\tau}^{\mathrm{T}} + \boldsymbol{L}^{\mathrm{T}}\big)\Phi, \quad \beta_2 = \cdots = \beta_N = 0,$$

which are the real parts of $\tilde{\lambda}_1, \dots, \tilde{\lambda}_N$ given by (2.14). We have proved the following lemma.

Lemma 2.1. *Under the assumption* (2.12)*, the stability criterion* (2.11) *is violated for a vector* $\Phi := \Phi^{(0)}$*, i.e. the matrix* $\boldsymbol{M}$ *has an eigenvalue* μ *with* $\operatorname{Re}\mu < 0$*, if and only if* $V'(\phi) < 0$ *and* $(v^{\max}\phi V'(\phi)\boldsymbol{\tau}^{\mathrm{T}} + \boldsymbol{L}^{\mathrm{T}})\Phi > 0$*, that is, if the matrix* $\boldsymbol{B}$ *has a negative eigenvalue* β_1*.*

3. Parabolicity analysis

We first quote some results from [12, 14] that are needed to establish the stability results of each of the convective and diffusive terms appearing in (1.6).

Theorem 3.1 ([14])**.** *Assume that the components of* $\boldsymbol{f}(\Phi)$ *are given by* (1.5)*, and that the velocities* $v_i^{\max}$ *are ordered according to* (2.1)*. If* $\Phi \in \mathcal{D}^0$*, then the Jacobian* $\mathcal{J}_{\boldsymbol{f}}(\Phi)$ *has* N *pairwise distinct real eigenvalues* $\lambda_1, \dots, \lambda_N$*, and the following interlacing property holds:*

$$v_N^{\max} + V'(\phi)(\boldsymbol{v}^{\max})^{\mathrm{T}}\Phi < \lambda_N < v_N^{\max} < \lambda_{N-1} < v_{N-1}^{\max} < \cdots < v_2^{\max} < \lambda_1 < v_1^{\max}.$$

Theorem 3.2 ([12])**.** *The eigenvalues of* $\boldsymbol{B}(\Phi)$ *are given by* $\mu_i = -V'(\phi)\lambda_i$*,* $i = 1, \dots, N$*, where*

$$\lambda_1 = \frac{C_1}{2} - \left(\frac{C_1^2}{4} - C_2\right)^{1/2}, \quad \lambda_2 = \frac{C_1}{2} + \left(\frac{C_1^2}{4} - C_2\right)^{1/2}, \quad \lambda_3 = \cdots = \lambda_N = 0,$$

where we define

$$C_1 = \sum_{k=1}^{N} \phi_k v_k^{\max}\big(L_k + \tau_k V'(\phi)(\boldsymbol{v}^{\max})^{\mathrm{T}}\Phi\big),$$
$$C_2 = \sum_{\substack{i,j=1 \\ i<j}}^{N} \phi_i v_i^{\max}\phi_j v_j^{\max}\tau_i\tau_j \left(\frac{L_i}{\tau_i} - \frac{L_j}{\tau_j} + (v_j^{\max} - v_i^{\max})V(\phi)\right)(v_j^{\max} - v_i^{\max})V(\phi). \tag{3.1}$$

A sufficient condition for $\boldsymbol{B}(\Phi)$ *to have eigenvalues with non-negative real parts only is that* $C_1, C_2 > 0$ *and* $C_1^2 \neq 4C_2$*.*

Since $C_1^2 \neq 4C_2$ generically, we henceforth use $C_1, C_2 > 0$ as a sufficient condition for $\boldsymbol{B}(\Phi)$ to have eigenvalues with non-negative real parts only. From the next result we can obtain reaction times that ensure that the matrix $\boldsymbol{B}(\Phi)$ has eigenvalues with non-negative real parts only with velocity functions $V(\phi)$ that satisfy

$$V(\phi) = \begin{cases} 1 & \text{for } \phi \le \phi_{\mathrm{c}}, \\ W(\phi) & \text{for } \phi > \phi_{\mathrm{c}}, \end{cases} \tag{3.2}$$

where W is a function that satisfies $W(\phi_c) = 1$, $W(1) = 0$ and $W'(\phi) < 0$ for $\phi_c < \phi < 1$. For instance, $W(\phi) = -C \ln \phi$ with $\phi_c = \phi_{DG}$ gives the Dick-Greenberg model (2.5) and $W(\phi) = (1-\phi)/(1-\phi_v)$ produces a variant of the Greenshields model (2.6).

Theorem 3.3. *Let $v_1^{\max}, \ldots, v_N^{\max}$ be free velocities such that $v_1^{\max} > v_2^{\max} > \cdots > v_N^{\max}$, $V(\phi)$ a velocity function that satisfies (3.2) and*

$$L_i = L_i(\phi) = \max\{L_{\min}, \beta(v_i^{\max} V(\phi))^2\}, \tag{3.3}$$

where the parameters $L_{\min}, \beta > 0$ are chosen such that

$$L_{\min} \leq \beta (v_i^{\max})^2. \tag{3.4}$$

Then there exist reaction times $\tau_i = \tau(v_i^{\max})$ for $i = 1, \ldots, N$, where $\tau(v)$ is a monotone increasing function and $\tau_1 \leq L_{\min}/(v_1^{\max}\kappa)$, with $\kappa = \max_\phi |\phi V'(\phi)|$, such that the matrix $\boldsymbol{B}(\Phi)$ has eigenvalues with positive real part.

Note that (3.3) is a multiclass version of the equation

$$L(\phi) = \max\left\{L_{\min}, \frac{(v(\phi))^2}{2a}\right\}$$

proposed in [23] for $N = 1$, where a is the deceleration and $L_{\min}$ is a minimum anticipation distance (regardless of how small the velocity is).

Proof of Theorem 3.3. We consider $\phi > \phi_c$, since $\boldsymbol{B}(\Phi) = 0$ otherwise. By Theorem 3.2 it is ensured that $\boldsymbol{B}(\Phi)$ has eigenvalues with non-negative real parts only when $C_1, C_2 > 0$, and this is in turn guaranteed when

$$L_k + \tau_k S(\Phi) \geq 0 \quad \text{for all } \Phi \text{ and } k = 1, \ldots, N, \quad S(\Phi) := V'(\phi)\Phi^{\mathrm{T}} \boldsymbol{v}^{\max}, \tag{3.5}$$

$$\Delta_{ij} := \frac{L_i}{\tau_i} - \frac{L_j}{\tau_j} + \big(v_j^{\max} - v_i^{\max}\big)V(\phi) \leq 0 \quad \text{for all } \Phi \text{ and } 1 \leq i < j \leq N. \tag{3.6}$$

Let $\phi = \phi_i^*$ be the unique solution of $L_{\min} = \beta (v_i^{\max})^2 V(\phi)^2$, then

$$L_i(\phi) = \begin{cases} \beta (v_i^{\max})^2 V(\phi)^2 & \text{for } \phi \leq \phi_i^*, \\ L_{\min} & \text{for } \phi \geq \phi_i^*. \end{cases} \tag{3.7}$$

From the assumption (3.4) we deduce that $\phi_c \leq \phi_i^*$ for $i = 1, \ldots, N$. Furthermore, $\phi_i^* \geq \phi_j^*$ for $i < j$. Moreover, $S(\Phi) = V'(\phi)\Phi^{\mathrm{T}}\boldsymbol{v}^{\max} \geq V'(\phi)\phi v_1^{\max}$ implies that a sufficient condition for (3.5) to hold is given by

$$\tau_i \leq \frac{L_{\min}}{\kappa v_1^{\max}} \quad \text{for } i = 1, \ldots, N. \tag{3.8}$$

We consider now condition (3.6). From (3.2) and (3.7) we get

$$\frac{L_i}{\tau_i} - v_i^{\max} V(\phi) = \begin{cases} \dfrac{\beta (v_i^{\max})^2}{\tau_i} - v_i^{\max} & \text{if } \phi \leq \phi_c, \\ \dfrac{\beta (v_i^{\max})^2 W(\phi)^2}{\tau_i} - v_i^{\max} W(\phi) & \text{if } \phi_c \leq \phi \leq \phi_i^*, \\ \dfrac{L_{\min}}{\tau_i} - v_i^{\max} W(\phi) & \text{if } \phi_i^* \leq \phi \leq 1, \end{cases} \quad i = 1, \ldots, N.$$

We consider a pair of indices $i < j$ and discuss the cases determined by ϕ belonging to $[\phi_c, \phi_j^*]$ (Case 1), $[\phi_j^*, \phi_i^*]$ (Case 2) or $[\phi_i^*, 1]$ (Case 3).

In Case 1, if we use the functional form $\tau_i = \tau(v_i^{\max})$, for some τ to be determined, and denote

$$\psi(v,\phi) := \frac{\beta(vW(\phi))^2}{\tau} - vW(\phi),$$

then $\Delta_{ij} = \psi(v_i^{\max},\phi) - \psi(v_j^{\max},\phi)$. If $\psi_v \le 0$ then $\Delta_{ij} \le 0$ for $i<j$, and this is equivalent to

$$\tau' \ge \frac{2\tau}{v} - \frac{\tau^2}{v^2\tilde{\beta}}, \quad \tilde{\beta} := \tilde{\beta}(\phi) := \beta W(\phi).$$

We consider $\mu(v) = v^n\tau(v)$, with n to be determined so to simplify the latter expression:

$$\mu' = nv^{n-1}\tau + v^n\tau' \ge nv^{n-1}\tau + v^n\left(\frac{2\tau}{v} - \frac{\tau^2}{v^2\tilde{\beta}}\right) = nv^{n-1}\tau + 2v^{n-1}\tau - \frac{v^{n-2}\tau^2}{\tilde{\beta}}.$$

We take $n=-2$ so that this expression yields:

$$\mu' \ge -\frac{v^{-4}\tau^2}{\tilde{\beta}} = -\frac{\mu^2}{\tilde{\beta}} \Longrightarrow \frac{\mu'}{\mu^2} = -\left(\frac{1}{\mu}\right)' \ge -\frac{1}{\tilde{\beta}} = -\left(\frac{v}{\tilde{\beta}}\right)',$$

and, upon integration and some algebra,

$$\tau = v^2\mu \ge \frac{\tilde{\beta}v^2}{v+\mathcal{A}}, \tag{3.9}$$

for some positive $\mathcal{A}$ to avoid null denominators.

In Case 2, and taking into account that $L_{\min} \ge \beta(v_j^{\max})^2W^2$ for $\phi \ge \phi_j^*$, we get

$$\begin{aligned}
\Delta_{ij} &= \frac{L_i}{\tau_i} - v_i^{\max}W(\phi) - \left(\frac{L_j}{\tau_j} - v_j^{\max}W(\phi)\right) \\
&= \frac{\beta(v_i^{\max})^2W(\phi)^2}{\tau_i} - v_i^{\max}W(\phi) - \left(\frac{L_{\min}}{\tau_j} - v_j^{\max}W(\phi)\right) \\
&\le \frac{\beta(v_i^{\max})^2W(\phi)^2}{\tau_i} - v_i^{\max}W(\phi) - \left(\frac{\beta(v_j^{\max})^2W(\phi)^2}{\tau_j} - v_j^{\max}W(\phi)\right),
\end{aligned}$$

As in Case 2, if τ satisfies (3.9) then $\Delta_{ij} \le 0$.

In Case 3 we get

$$\begin{aligned}
0 &\ge \frac{L_{\min}}{\tau_i} - v_i^{\max}W(\phi) - \left(\frac{L_{\min}}{\tau_j} - v_j^{\max}W(\phi)\right) \\
&= L_{\min}\left(\frac{1}{\tau_i} - \frac{1}{\tau_j}\right) - W(\phi)\left(v_i^{\max} - v_j^{\max}\right).
\end{aligned} \tag{3.10}$$

Since $W(1)=0$ and $v_i^{\max} > v_j^{\max}$, then (3.10) holds if and only if $\tau_i \ge \tau_j$.

Recapitulating, we deduce that (3.6) holds if $\tau_i = \tau(w_i)$ with τ satisfying

$$\tau \ge \frac{\beta W(\phi)v^2}{v+\mathcal{A}}, \quad \text{for all } \phi, \quad \tau' \ge 0,$$

and, since $W(\phi) \le 1$, this is equivalent to

$$\tau \ge \frac{\beta v^2}{v+\mathcal{A}}, \quad \tau' \ge 0. \tag{3.11}$$

We consider the increasing function

$$\tilde{\tau}(v) := \frac{\beta v^2}{v + \mathcal{A}}$$

for $\mathcal{A} > 0$ that certainly satisfies (3.11). Therefore, to ensure that $\boldsymbol{B}(\Phi)$ with $\tau_i = \tilde{\tau}(w_i)$ has eigenvalues with non-negative real parts only, we use (3.8), so we need to find conditions on $\mathcal{A}$ so that

$$\frac{\beta v^2}{v + \mathcal{A}} \leq \frac{L_{\min}}{\kappa v_1^{\max}} \Longleftrightarrow \beta v^2 - \frac{L_{\min}}{\kappa v_1^{\max}}(v + \mathcal{A}) \leq 0 \quad \text{for all } 0 \leq v \leq v_1^{\max}. \tag{3.12}$$

The roots of

$$\beta v^2 - \frac{L_{\min}}{\kappa v_1^{\max}}(v + \mathcal{A}) = 0$$

are

$$w_{\pm} = \frac{1}{2\beta}\left[\frac{L_{\min}}{\kappa v_1^{\max}} \pm \left(\left(\frac{L_{\min}}{\kappa v_1^{\max}}\right)^2 + 4\beta \frac{L_{\min}}{\kappa v_1^{\max}}\mathcal{A}\right)^{1/2}\right]$$

and (3.12) will hold if $w_- \leq 0$ (which is true) and $v_1^{\max} \leq w_+$, which yields after some algebraic manipulations

$$\beta (v_1^{\max})^2 \leq \frac{L_{\min}}{\kappa} + \frac{L_{\min}}{\kappa v_1^{\max}}\mathcal{A} \Longrightarrow \mathcal{A} \geq \left(\frac{\kappa \beta (v_1^{\max})^2}{L_{\min}} - 1\right) v_1^{\max} > 0.$$

This concludes the proof. □

4. Numerical examples

In the subsequent series of examples, we solve the system (1.6) numerically for $0 \leq t \leq T$ and $0 \leq x < \mathcal{L}$ along with the initial and periodic boundary conditions

$$\Phi(x, 0) = \Phi_0(x), \quad 0 \leq x < \mathcal{L}; \quad \Phi(0, t) = \Phi(\mathcal{L}, t) \quad \text{for } 0 \leq t \leq T,$$

corresponding to a circular one-directional road of length $\mathcal{L}$. Numerical approximations are obtained by the Kurganov-Tadmor (KT) scheme [19] applied to the DCMCLWR model. In fact, Kurganov and Tadmor [19] explicitly propose a version of their scheme for convection-diffusion problems of the type (1.6), even though a well-posedness analysis for systems of PDEs of this type is not available in the strongly degenerate case. In [5] the same method was applied to (1.6) in the context of a model of polydisperse sedimentation. To further support the use of the KT scheme, we mention that numerical experiments conducted in [12] indicate that the KT scheme and an alternative implicit-explicit (IMEX) scheme designed for (1.6) that involves a spectral WENO scheme for the convective part converge to the same solution of (1.6) as $\Delta t, \Delta x \to 0$ (under suitable CFL conditions). In some examples we will compare the performance of the KT scheme with that of one of the schemes introduced in [12], namely the scheme IMEX-RK(3,4,3).

In the following numerical examples, and unless otherwise stated, the x-interval $[0, \mathcal{L}]$ is subdivided into $M = 3200$ subintervals of length $\Delta x = \mathcal{L}/M$. We denote by Δt the time step used to advance the numerical solution from time $t = t_n$ to $t_{n+1} = t_n + \Delta t$ and by Φ_j^n the vector of numerical solutions associated with cell $[j\Delta x, (j+1)\Delta x)$, $j = 0, \ldots, M-1$, at time t_n. For each iteration, the time step Δt

is determined anew by using the following formula (derived from a linearized CFL condition):

$$\frac{\Delta t}{\Delta x}\max_{0\le j\le M-1}\varrho\big(\mathcal{J}_{\boldsymbol{f}}(\Phi_j^n)\big)+\frac{\Delta t}{2\Delta x^2}\max_{0\le j\le M-1}\varrho\big(\boldsymbol{B}(\Phi_j^n)\big)=C_{\mathrm{cfl}},$$

where $\varrho(\cdot)$ is the spectral radius. In the numerical examples we choose C_{cfl} as the largest multiple of 0.05 that yields oscillation-free numerical solutions when these are expected to be so.

Finally, in some of the examples we present approximate L^1 errors to illustrate the convergence properties of the numerical scheme. As in [12], these approximate errors are computed as follows: Let us denote by $(\phi_{j,i}^M(t))_{j=1}^M$ and $(\phi_{l,i}^{\mathrm{ref}}(t))_{l=1}^{M_{\mathrm{ref}}}$ the numerical solution for the i-th component at time t calculated with M and M_{ref} cells, respectively. We use cubic interpolation from the reference grid to the M cells grid to compute $\widetilde{\phi}_{j,i}^{\mathrm{ref}}(t)$ for $j=1,\dots,M$. We then calculate the approximate L^1 error of class i by

$$e_i(t):=\frac{1}{M}\sum_{j=1}^{M}\big|\widetilde{\phi}_{j,i}^{\mathrm{ref}}(t)-\phi_{j,i}^M(t)\big|,\quad i=1,\dots,N.$$

We define the total approximate L^1 error at time t as $e_{\mathrm{tot}}(t):=e_1(t)+\cdots+e_N(t)$.

4.1. **Example 1 (DG model, $N=4$, stable behaviour).** In Example 1 we consider the DG velocity function (2.5), a circular road of length $\mathcal{L}=10\,\mathrm{mi}$, $N=4$ driver classes with the respective preferential velocities $v_1^{\max}=60\,\mathrm{mi/h}$, $v_2^{\max}=55\,\mathrm{mi/h}$, $v_3^{\max}=50\,\mathrm{mi/h}$ and $v_4^{\max}=45\,\mathrm{mi/h}$, and a uniform minimum anticipation length $L_{\min}=0.03\,\mathrm{mi}$. The reaction times are chosen such that the eigenvalues of the diffusion matrix $\boldsymbol{B}(\Phi)$ have non-negative real parts for $\Phi\in\mathcal{D}^0\subset\mathbb{R}^4$. According to (3.1) this is ensured if the parameters $\tau_1,\dots,\tau_N$ satisfy the following condition:

$$\tau_1\le\frac{L_{\min}}{Cv_1^{\max}};\quad \tau_i\le\left(\frac{v_i^{\max}}{v_{i-1}^{\max}}\right)^2\tau_{i-1},\quad i=2,\dots,N. \tag{4.1}$$

To satisfy (4.1) here, we choose $\tau_1=0.0013\,\mathrm{h}$, $\tau_2=0.0011\,\mathrm{h}$, $\tau_3=0.0008\,\mathrm{h}$ and $\tau_4=0.0006\,\mathrm{h}$. Figure 1 shows the evolution of the initial traffic "platoon" given by

$$\Phi_0(x,0)=p(x)\begin{pmatrix}0.2\\0.3\\0.2\\0.3\end{pmatrix},\quad p(x)=\begin{cases}10x & \text{for } 0<x\le 0.1,\\ 1 & \text{for } 0.1<x\le 0.9,\\ -10(x-1) & \text{for } 0.9<x\le 1,\\ 0 & \text{otherwise.}\end{cases} \tag{4.2}$$

We observe that the system tends to a stationary constant solution.

4.2. **Examples 2–5 (DG model, $N=2$, unstable behaviour).** In Examples 2 to 5 we consider the DG model (2.5), a circular road of length $\mathcal{L}=2\,\mathrm{mi}$, and $N=2$ driver classes. The preferential velocities of the two classes are given by $v_1^{\max}=80\,\mathrm{mi/h}$ and $v_2^{\max}=30\,\mathrm{mi/h}$, and a minimum anticipation distance $L_{\min}=0.03\,\mathrm{mi}$. For Example 2, the parameters $\tau_1=0.00096\,\mathrm{h}$ and $\tau_2=0.0025\,\mathrm{h}$ have been chosen in such a way that the condition for the PDE (1.3) (for $N=1$) to be parabolic for $\phi>\phi_{\mathrm{c}}$, namely

$$\tau\le\frac{L}{|\phi V'(\phi)|v^{\max}}\quad\text{for } \phi_{\mathrm{c}}\le\phi<1, \tag{4.3}$$

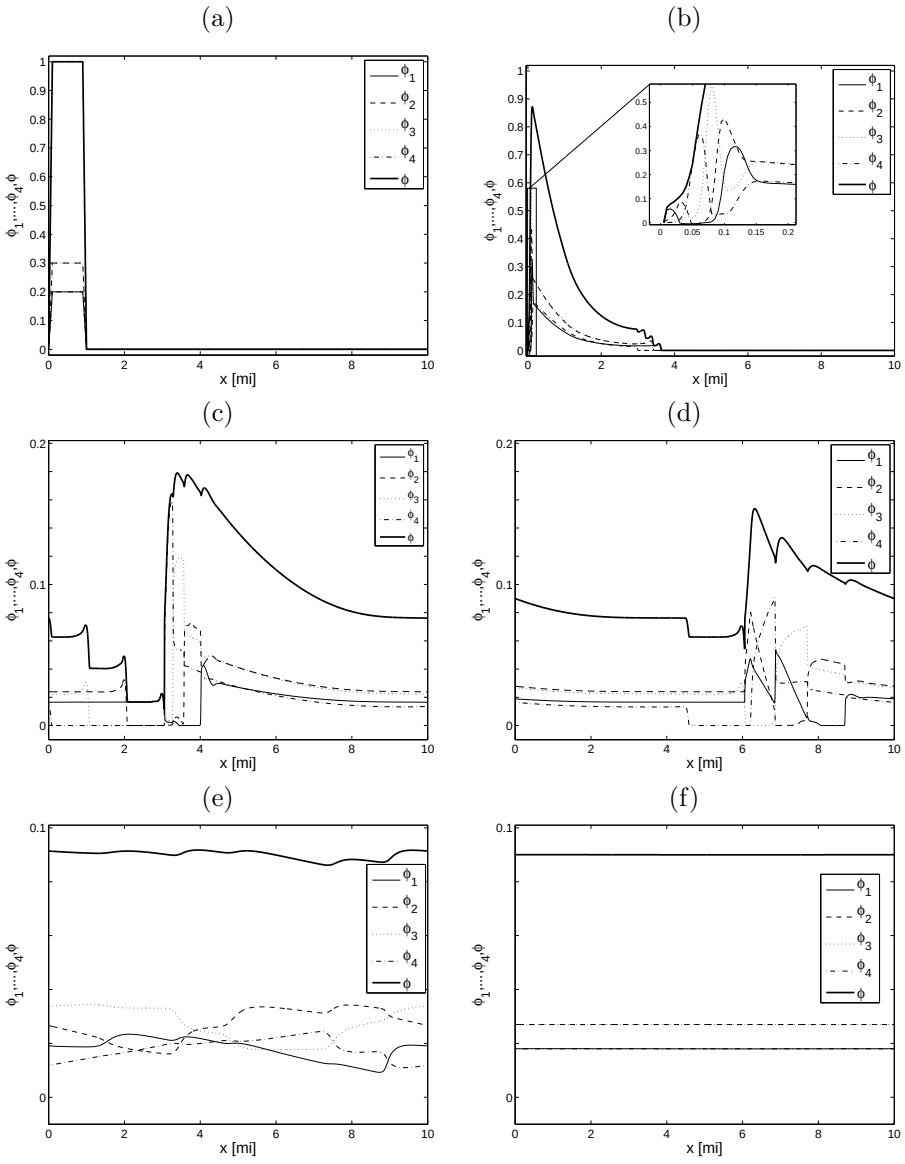

FIGURE 1. Example 1 (DG model, $N = 4$): (a) initial datum (4.2) and (b–f) numerical solution at simulated times (b) $t = 0.08\,\mathrm{h}$, (c) $t = 0.2\,\mathrm{h}$, (d) $t = 0.3\,\mathrm{h}$, (e) $t = 9\,\mathrm{h}$ and (f) $T = 50.0\,\mathrm{h}$.

is satisfied by both triples $(v^{\max}, L, \tau) = (v_i^{\max}, L_i, \tau_i)$, $i = 1, 2$, but that at the same time $C_2 < 0$ in a subregion of $\mathcal{D}^0$. In Figure 2 we show a numerical example obtained for these values of parameters in which ϕ_1 and ϕ_2 initially have disjoint support, i.e. drivers of both classes are well separated. The "convoys" of both species initially evolve according to the scalar model studied in [8, 22, 23], see Figures 2 (a–c). As soon as both classes enter in contact, unstable solution behaviour emerges, as can be seen in the oscillatory part of the solution visible in Figure 2 (d).

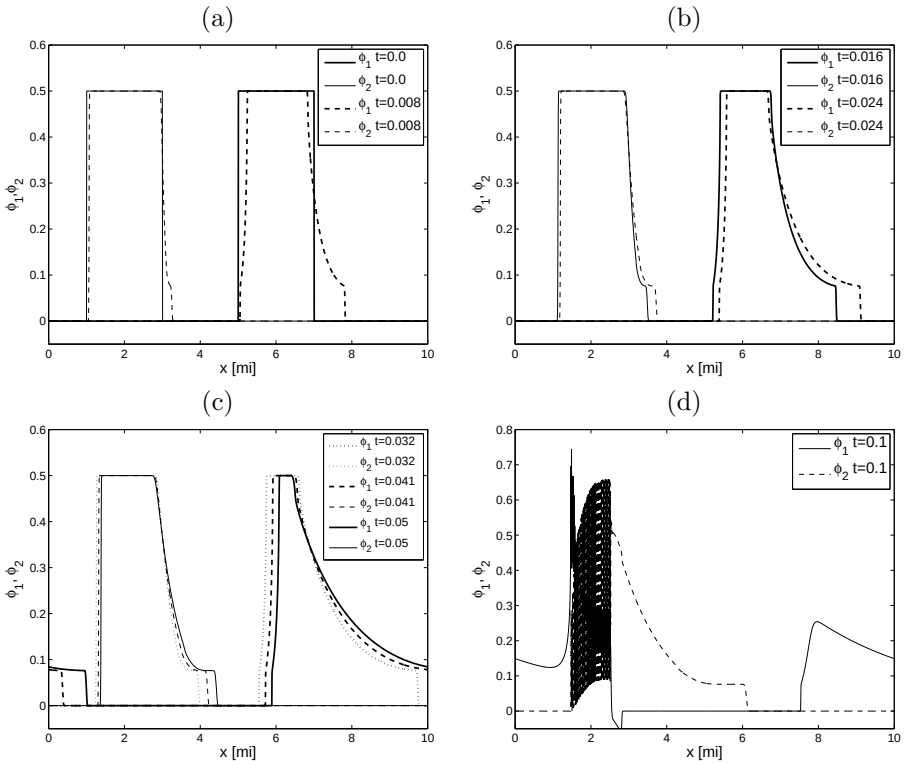

FIGURE 2. Example 2 (DG model, $N = 2$): (a, b, c) stable behaviour for individual driver classes (spatially separated), followed by (d) unstable behavior for mixed driver classes.

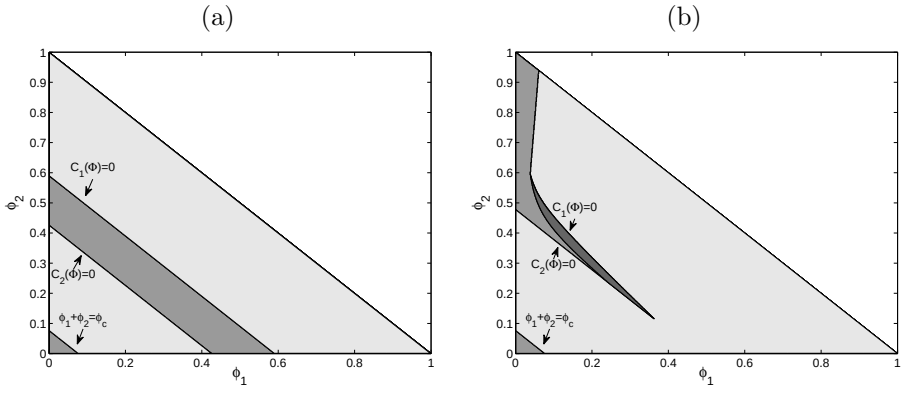

FIGURE 3. Examples 2–8 (DG model, $N = 2$). Stability region for the diffusion matrix $\boldsymbol{B}$ and instability region for $\boldsymbol{M}$ for $\xi \in [0, 100]$ for (a) Examples 2–5, (b) Examples 6–8.

To ensure the parabolicity condition, we choose reaction times according to (4.1) by setting $\tau_1 = 0.0008\,\mathrm{h}$ and $\tau_2 = 0.0011\,\mathrm{h}$ in Examples 3–5. As in Example 2, we

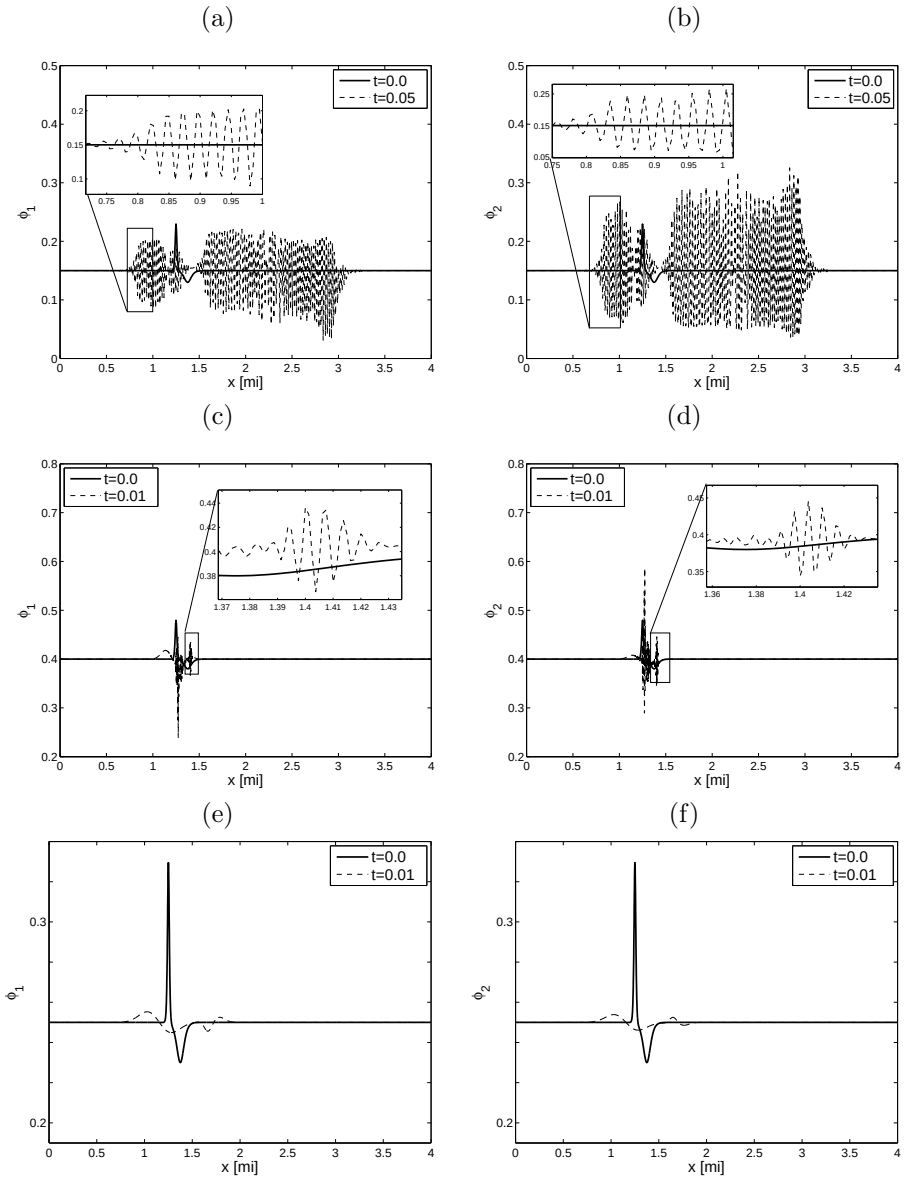

FIGURE 4. Examples 3–5 (DG model, $N = 2$): Simulations for different initial conditions which lie in the stability or instability region (cf. Figure 3): (a, b) $\phi_1^0 = \phi_2^0 = 0.15$ (Example 3), (c, d) $\phi_1^0 = \phi_2^0 = 0.4$ (Example 4), (e, f) $\phi_1^0 = \phi_2^0 = 0.25$ (Example 5).

observe that with these reaction times each driver class is associated with stable behaviour when the respective other class is absent. In Figure 3 (a) we describe a stability region in the (ϕ_1, ϕ_2)-plane (phase space) corresponding to points at which the real parts of the eigenvalues of $\boldsymbol{B}(\Phi)$ are positive. This is a subregion of $\mathbb{R}^2_+$

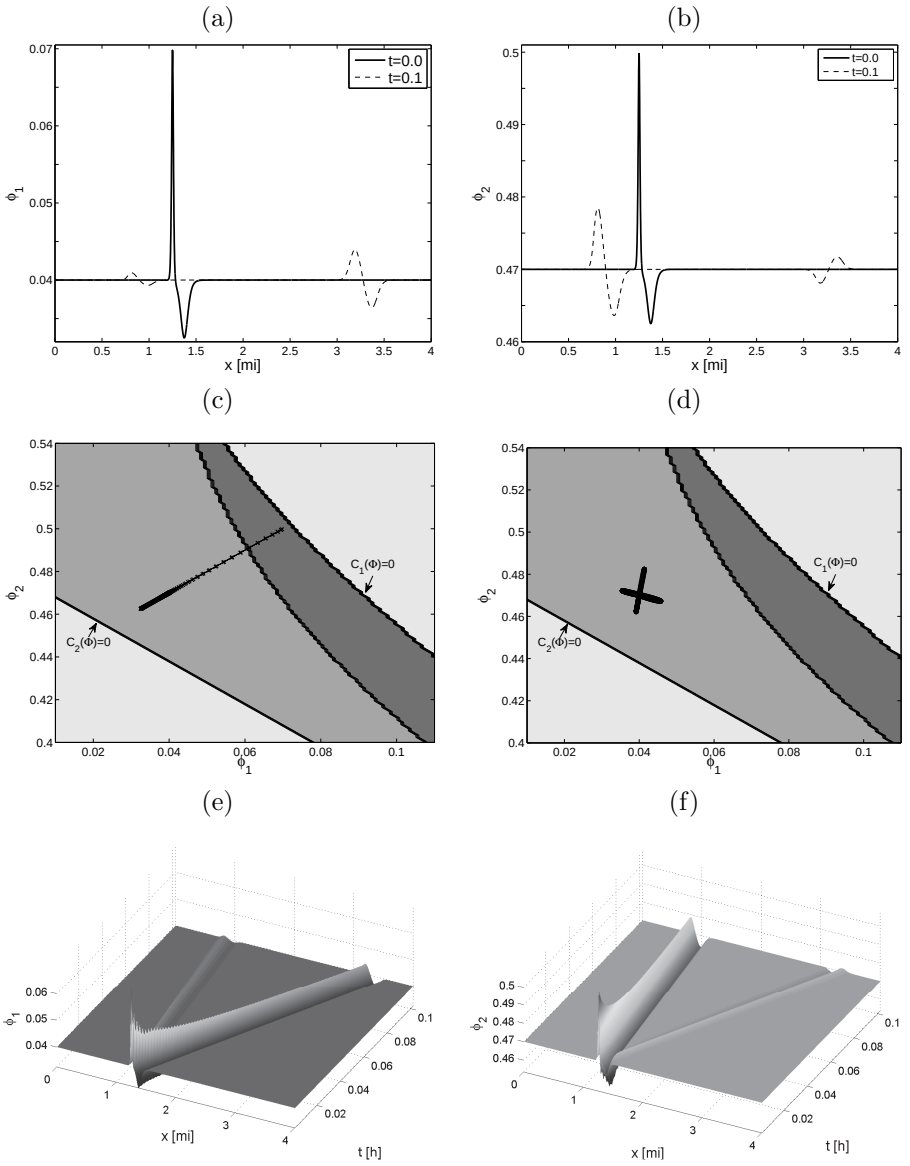

FIGURE 5. Example 6 (DG model, $N = 2$). Unperturbed initial state in stability region of $\boldsymbol{B}$ and initial perturbation in stability region of $\boldsymbol{B}$ and partially in instability region of $\boldsymbol{M}$: (a, b) initial datum and numerical solution at $t = 0.1$ h; (c, d) phase plane plots of (c) the initial datum and (d) the numerical solution for $t = 0.1$ h; (e, f) numerical solution for $0 \le t \le 0.1$ h.

bounded by curves $C_1(\Phi) = 0$ and $C_2(\Phi) = 0$. Next, we choose the initial condition

$$\phi_i(x,0) = \phi_i^0 + \delta\phi^0 \left[\cosh^{-2}\left(\frac{320}{\mathcal{L}}\left(x - \frac{5\mathcal{L}}{16}\right)\right) - 0.25\cosh^{-2}\left(\frac{40}{\mathcal{L}}\left(x - \frac{11\mathcal{L}}{32}\right)\right)\right] \tag{4.4}$$

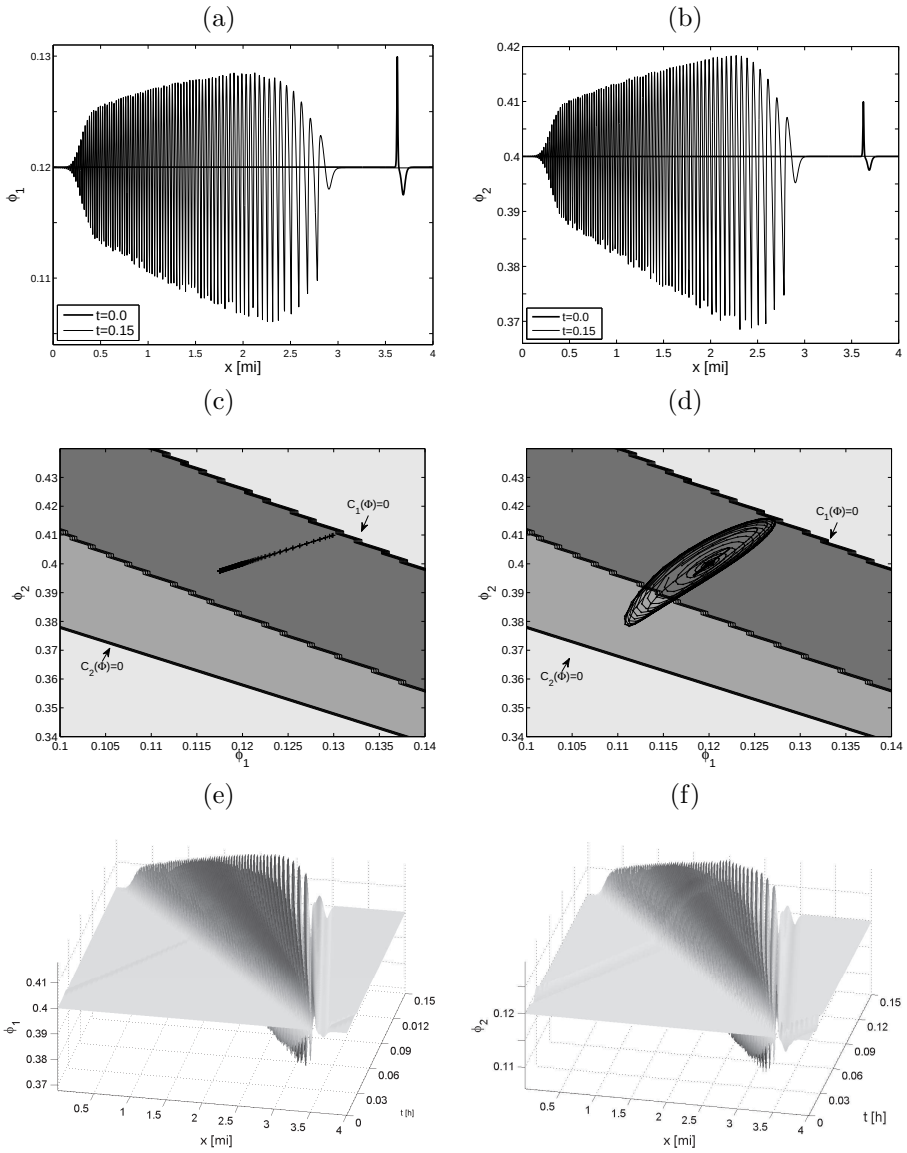

FIGURE 6. Example 7 (DG model, $N = 2$). Unperturbed initial state and initial perturbation in stability region of $\boldsymbol{B}$ and in instability region of $\boldsymbol{M}$: (a, b) initial datum and numerical solution at $t = 0.1\,\mathrm{h}$; (c, d) phase plane plots of (c) the initial datum and (d) the numerical solution for $t = 0.1\,\mathrm{h}$; (e, f) numerical solution for $0 \le t \le 0.1\,\mathrm{h}$.

for $i = 1, 2$ (similar to the one proposed in [27]), where $\delta\phi^0$ is the amplitude of perturbation; we here choose $\delta\phi^0 = 0.08$. We select the initial density Φ^0 in the different regions and compute the solution until a finite time. For the initial conditions $\phi_1^0 = \phi_2^0 = 0.15$ (Example 3) or $\phi_1^0 = \phi_2^0 = 0.4$ (Example 4) (Figures 4 (a–d)),

	IMEX-RK(3,4,3)		KT	
M	error	CPU time [s]	error	CPU time [s]
400	1.7e-3	1.92	1.8e-3	2.29
800	1.4e-3	6.60	1.7e-3	9.92
1600	9.3e-4	25.74	1.2e-3	55.94
3200	2.9e-4	105.91	8.9e-4	308.26

TABLE 1. Example 7 (DG model, $N = 2$): approximate total L^1 errors and CPU times at time $t = 0.03$ h for the KT scheme with $C_{\text{cfl1}} = 0.1$ and scheme IMEX-RK(3,4,3) [12] with $C_{\text{cfl}} = 0.6$.

	IMEX-RK(3,4,3)		KT	
M	error	CPU time [s]	error	CPU time [s]
400	3.1e-4	2.52	4.9e-4	4.05
800	1.2e-4	10.60	2.4e-4	16.82
1600	5.3e-5	39.43	8.9e-5	87.65
3200	2.3e-5	145.04	2.8e-5	490.67

TABLE 2. Example 8 (DG model, $N = 2$): approximate total L^1 errors and CPU times at time $t = 0.03$ h for the KT scheme KT with $C_{\text{cfl1}} = 0.1$ and scheme IMEX-RK(3,4,3) [12] with $C_{\text{cfl}} = 0.6$.

	IMEX-RK(3,4,3)		KT	
M	error	CPU time [s]	error	CPU time [s]
400	21.4e-4	2.12	24.9e-4	4.05
800	18.3e-4	9.12	20.3e-4	67.80
1600	14.1e-4	47.38	18.9e-4	274.75
3200	7.23e-5	205.44	10.3e-4	1059.48

TABLE 3. Example 10 (GS model, $N = 2$): approximate total L^1 errors and CPU times at time $t = 0.03$ h for the KT scheme with $C_{\text{cfl1}} = 0.05$ and scheme IMEX-RK(3,4,3) [12] with $C_{\text{cfl}} = 0.6$.

i	1	2	3	4	5
L_i [mi]	0.006	0.012	0.03	0.008	0.028
τ_i [h]	0.00028	0.00052	0.00132	0.00036	0.00122

TABLE 4. Example 12 (DG model, $N = 5$, drivers having the same maximum speed): reaction times and anticipation distances.

which lie both in the instability region, we observe that amplitudes present in the initial datum are expanded but remain bounded in the instability region, while the frequencies are extended to maximum frequency. When $\phi_1^0 = 0.25$ and $\phi_2^0 = 0.25$ in the stability region (Example 5), simulations (Figures 4 (e, f)) show that amplitudes of the disturbance decrease with time, and that the corresponding frequency

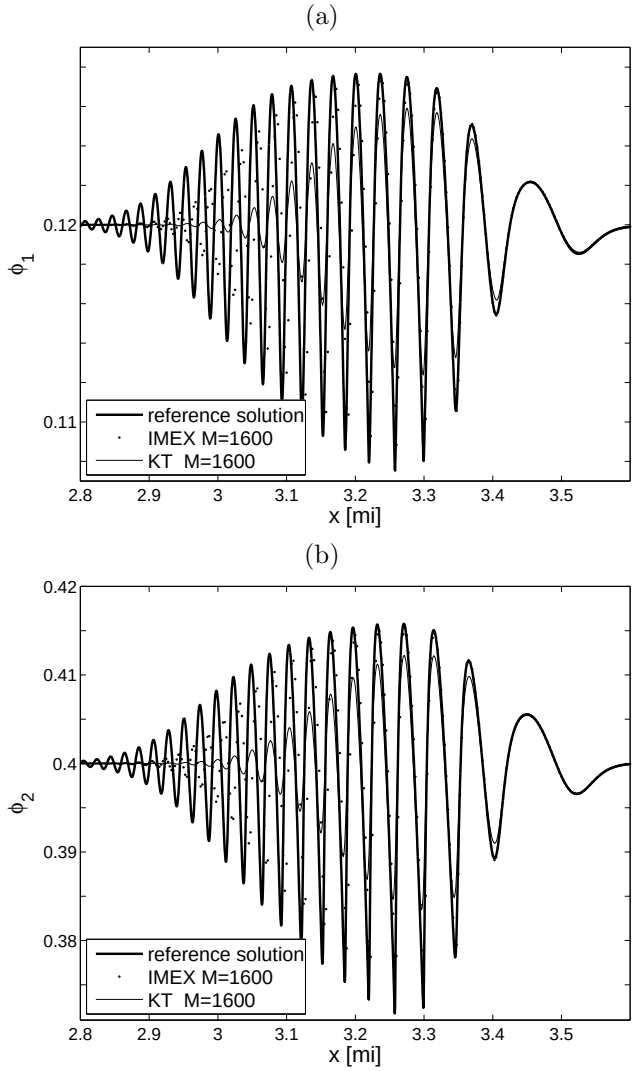

FIGURE 7. Example 7 (DG model, $N = 2$): comparison of reference solution ($M_{\text{ref}} = 12800$) with approximate solutions computed by schemes KT and IMEX-RK(3,4,3) [12] with $M = 1600$.

of oscillation does not increase. In both cases, initial perturbations generate waves traveling downstream and upstream.

4.3. **Examples 6–8 (DG model, $N = 2$, mildly unstable behaviour).** We continue using the DG model (2.5), consider a circular road of length $\mathcal{L} = 4\,\text{mi}$ and employ $v_1^{\max} = 80\,\text{mi/h}$, $v_2^{\max} = 30\,\text{mi/h}$, $\tau_1 = 0.00095\,\text{h}$, $\tau_2 = 0.00075\,\text{h}$ and $L_{\min} = 0.01\,\text{mi}$. For this choice of parameters, we observe in Figure 3 (b) that the instability region of $\boldsymbol{M} = \boldsymbol{M}(\Phi, \xi)$ is a subset of the stability region of $\boldsymbol{B}$, which indicates that bounded or unbounded instabilities could be generated even when the parabolicity conditions (3.1) are satisfied. As in the last example, we choose

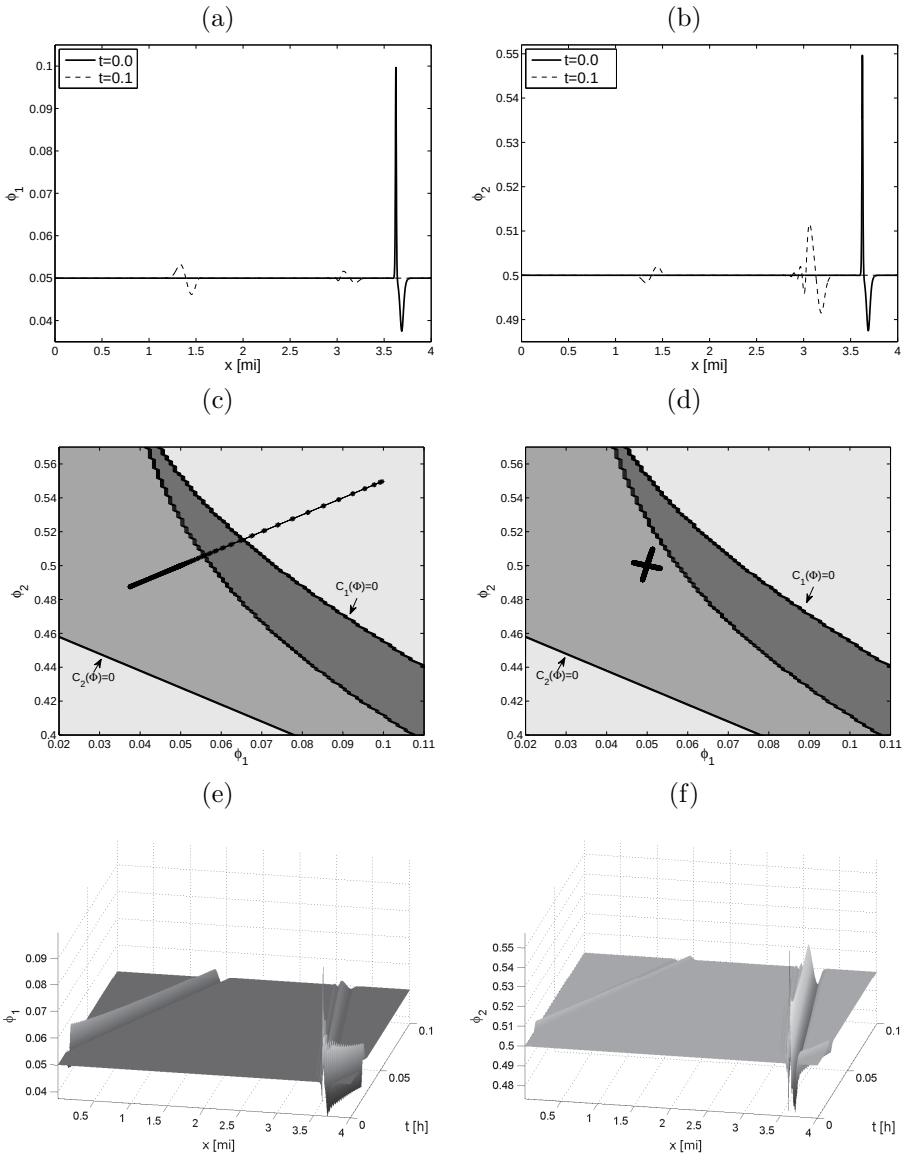

FIGURE 8. Example 8 (DG model, $N = 2$). Unperturbed initial state in stability region of $\boldsymbol{B}$ and large-amplitude initial perturbation partially in instability region of $\boldsymbol{B}$: (a, b) initial datum and numerical solution at $t = 0.1\,\mathrm{h}$; (c, d) phase plane plots of (c) the initial datum and (d) numerical solution for $t = 0.1\,\mathrm{h}$; (e, f) numerical solution for $0 \le t \le 0.1\,\mathrm{h}$.

two initial conditions close to the instability region. We display numerical solutions for different initial conditions. We observe in Figure 5 that an initial perturbation is split into two waves, a wave traveling downstream which decreases rapidly in amplitude, and another wave traveling upstream which can cause traffic instability

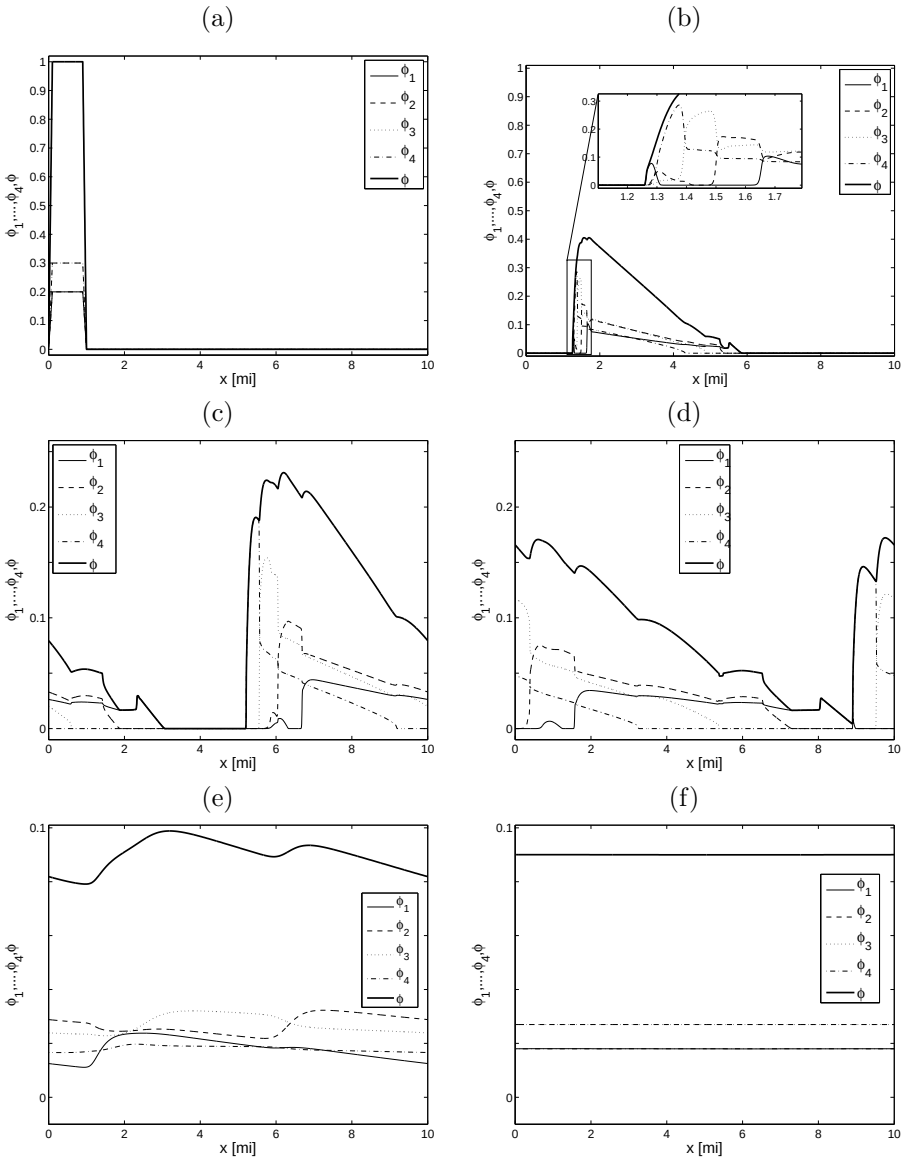

FIGURE 9. Example 9 (GS model, $N = 4$): (a) initial datum and solution at simulated times (b) $t = 0.08\,\mathrm{h}$, (c) $t = 0.2\,\mathrm{h}$, (d) $t = 0.3\,\mathrm{h}$, (e) $t = 9\,\mathrm{h}$ and (f) $t = T = 50.0\,\mathrm{h}$.

depending on the initial condition. For $\phi_1^0 = 0.04$ and $\phi_2^0 = 0.47$ (Example 6) and an initial perturbation with amplitude $\delta\phi^0 = 0.03$ which does not lie in the instability region for $\boldsymbol{M}$, waves traveling upstream and downstream decrease in amplitude until a steady state is nearly reached. Numerical solutions are displayed in Figure 5.

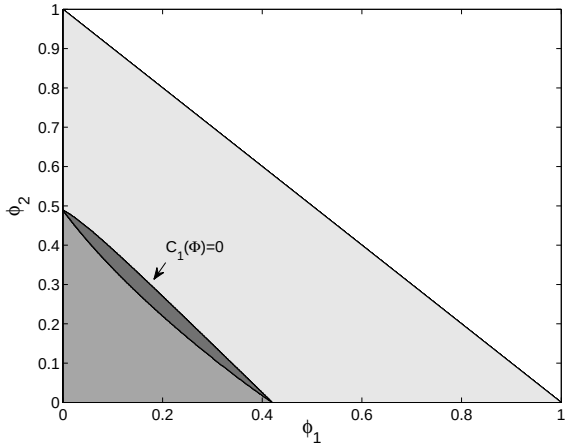

FIGURE 10. Examples 10 and 11 (GS model, $N = 2$): stability region for diffusion matrix $\boldsymbol{B}$ and instability region for $\boldsymbol{M}$.

For $\phi_1^0 = 0.12$ and $\phi_2^0 = 0.4$ (Example 7) and an initial perturbation with amplitude $\delta\phi^0 = 0.01$, which lie in the instability region for $\boldsymbol{M}$, waves traveling downstream decrease in amplitude, while waves traveling upstream grow in amplitude and until some frequency, which cause traffic instabilities. Numerical solutions at different times are displayed in Figure 6. Phase space diagrams are also shown in order to display how instabilities may be triggered. In Table 1 we calculate total approximate L^1 errors and CPU times at time $t = 0.03\,\mathrm{h}$ for two different numerical schemes. The reference solution was calculated using the KT scheme with $M = 12800$ subintervals. This information indicates that the numerical solutions produced by both schemes converge to the same solution as $\Delta t, \Delta x \to 0$. In particular, the oscillations visible in the numerical solution (see Figure 6 (a, b)) are not artifacts produced by the numerical scheme.

In Example 8 we choose the constants $\phi_1^0 = 0.05$ and $\phi_2^0 = 0.5$, which lie in the stability region, and add an initial perturbation with amplitude $\delta\phi^0 = 0.05$ so that the initial function $(\phi_1(x,0), \phi_2(x,0))^{\mathrm{T}}$ defined by (4.4) assumes values that are in the instability region for $B(\Phi)$. In the numerical solution (see Figure 8) we observe that waves traveling upstream generate a wave that decreases in amplitude, and we also observe instabilities that remain controlled. In Table 2 we calculate total approximate L^1 errors and CPU times at time $t = 0.03\,\mathrm{h}$ for two different numerical schemes. This table indicates that oscillations present in the numerical solution (cf. Figures 8 (a) and (b)) are not produced by the numerical scheme. That the oscillations are not a numerical artifact is further supported by Figure 7, where we compare the numerical solutions obtained for $M = 1600$ with both schemes with the reference solution, obtained by the KT scheme with $M_{\mathrm{ref}} = 12800$.

4.4. **Examples 9–11 (GS model, $N = 4$ and $N = 2$).** Now, we consider a DCMCLWR model with the Greenshields (GS) velocity function (2.6) and assume that $\boldsymbol{B}(\Phi)$ is given by (2.7) with the perception threshold $\phi_{\mathrm{c}} = 0.05$. In Example 9 we choose $N = 4$ and $v_1^{\max} = 60\,\mathrm{mi/h}$, $v_2^{\max} = 55\,\mathrm{mi/h}$, $v_3^{\max} = 50\,\mathrm{mi/h}$, $v_4^{\max} = 45\,\mathrm{mi/h}$ and $L_{\min} = 0.03\,\mathrm{mi}$. The reaction times are chosen such that the

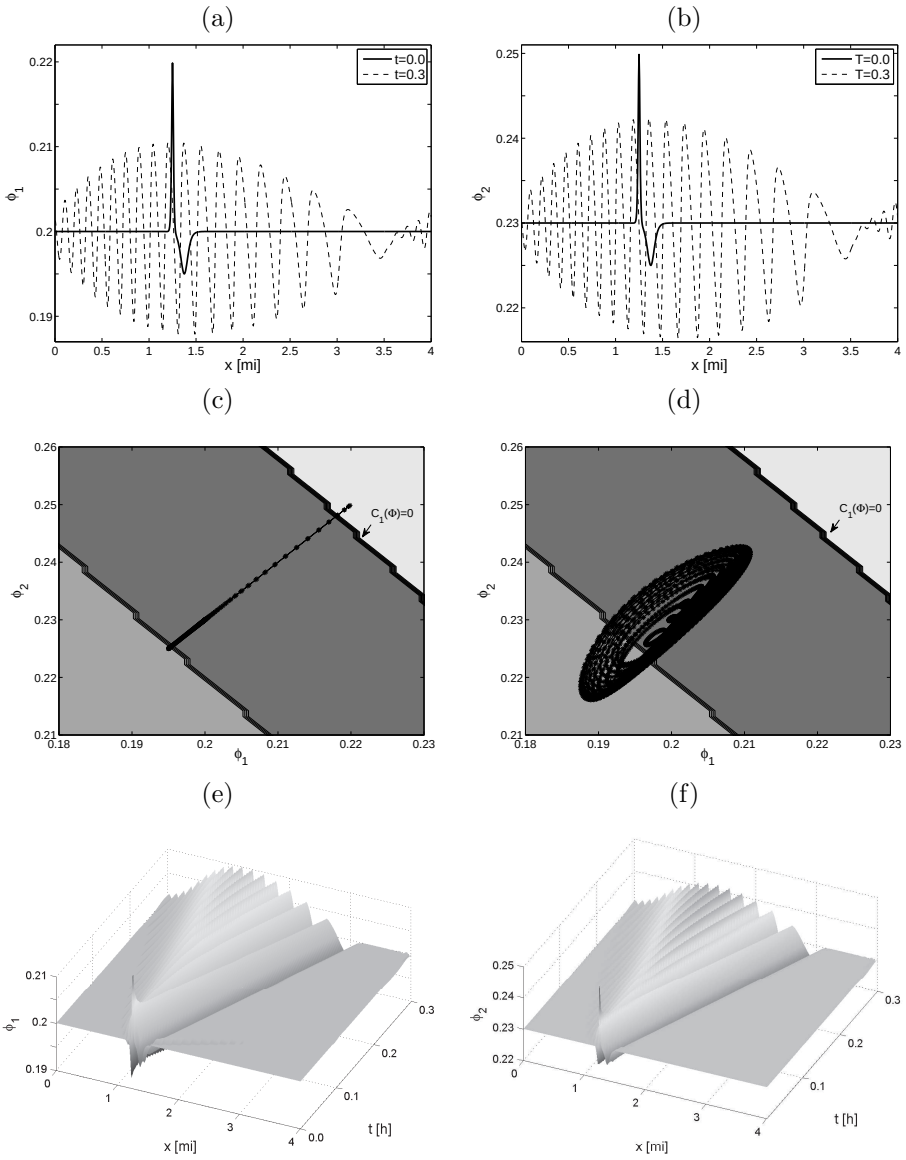

FIGURE 11. Example 10 (GS model, $N = 2$). Unperturbed initial state and small-amplitude initial perturbation in stability region of $\boldsymbol{B}$ and in instability region of $\boldsymbol{M}$: (a, b) initial datum and numerical solution at $t = 0.1\,\mathrm{h}$; (c, d) phase plane plots of (c) the initial datum and (d) the numerical solution for $t = 0.1\,\mathrm{h}$; (e, f) numerical solution for $0 \le t \le 0.1\,\mathrm{h}$.

eigenvalues of $\boldsymbol{B}(\Phi)$ have positive sign. In fact, we ensure that (3.1) holds by choosing $\tau_1 = 0.0005\,\mathrm{h}$, $\tau_2 = 0.0004\,\mathrm{h}$, $\tau_3 = 0.0003\,\mathrm{h}$ and $\tau_4 = 0.0002\,\mathrm{h}$. Figure 9 shows a time evolution of the initial concentration platoon to a final (nearly) constant steady state reached at $t = 50\,\mathrm{h}$.

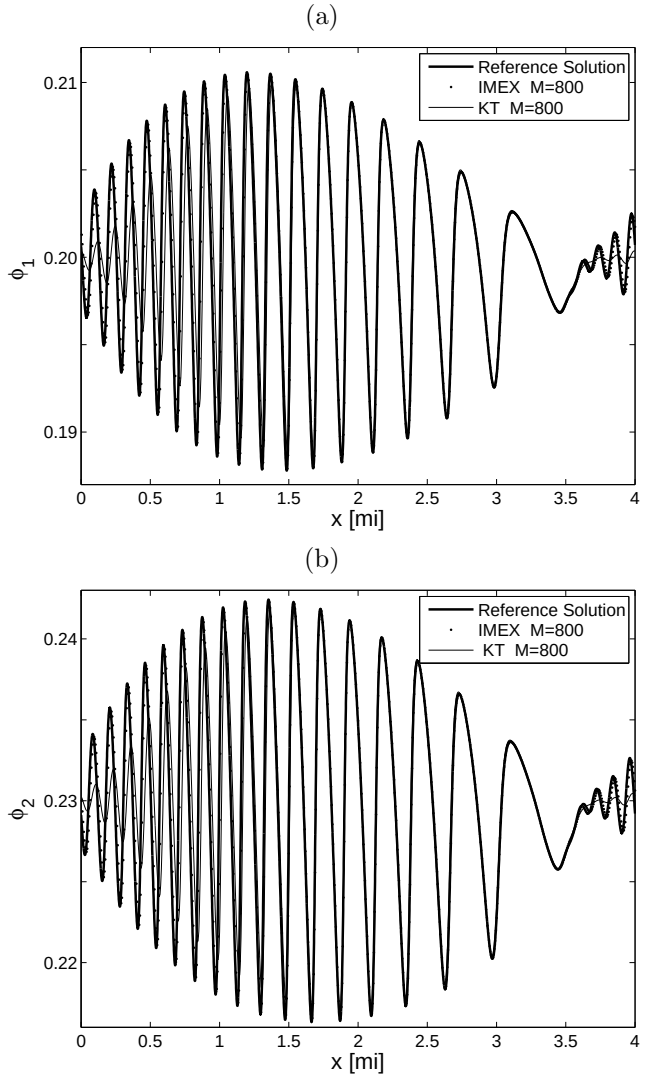

FIGURE 12. Example 10 (GS model, $N = 2$): comparison of reference solution ($M_{\text{ref}} = 12800$) with approximate solutions computed by schemes KT and IMEX-RK(3,4,3) [12] with $M = 800$.

To analyze chaotic behaviour, we consider in Example 10 a circular road of 4mi. and interaction between $N = 2$ classes with the respective free velocities $v_1^{\max} = 60\,\text{mi/h}$ and $v_2^{\max} = 30\,\text{mi/h}$ with an anticipation distance $L_{\min} = 0.01\text{mi}$. Instabilities occur when we choose reaction times as $\tau_1 = 0.0024\,\text{h}$ and $\tau_2 = 0.0008\,\text{h}$. In Figure 10 we display the stability region for the diffusion matrix $B(\Phi)$ and the instability region for the matrix $\boldsymbol{M}$. As for the Dick-Greenberg model, we choose two different initial conditions and show that traffic instabilities can occur. In Figure 11 we display a time evolution of an initial condition with $\phi_1 = 0.2$ and $\phi_2 = 0.23$ and a perturbation with amplitude $\delta\phi^0 = 0.02$ in the instability region

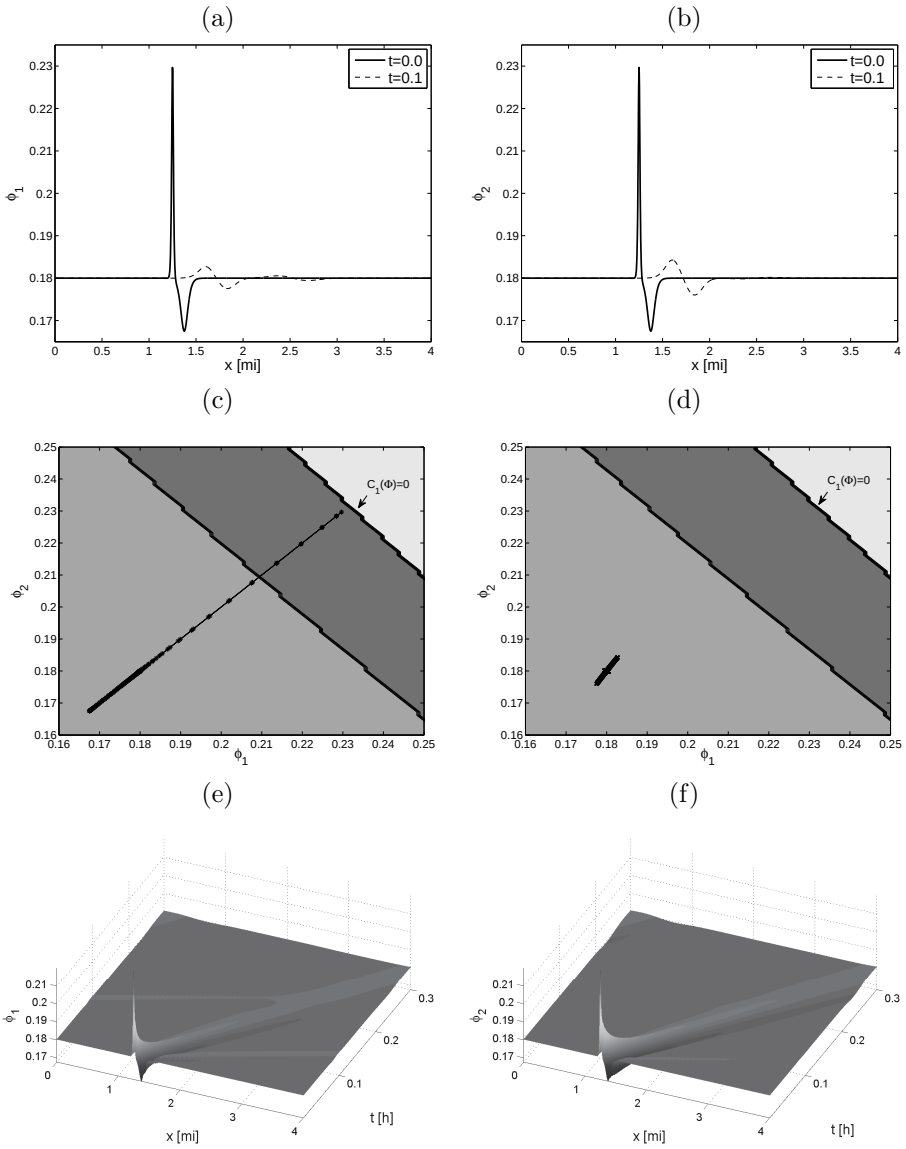

FIGURE 13. Example 11 (GS model, $N = 2$): Unperturbed initial state in stability region of $\boldsymbol{B}$ and initial perturbation in stability region of $\boldsymbol{B}$ and in instability region of $\boldsymbol{M}$: (a, b) initial datum and numerical solution at $t = 0.1\,\mathrm{h}$; (c, d) phase plane plots of (c) the initial datum and (d) the numerical solution for $t = 0.1\,\mathrm{h}$; (e, f) numerical solution for $0 \leq t \leq 0.1\,\mathrm{h}$.

(Example 10). We observe that the solution is a wave traveling upstream which grows in amplitude and frequency. We also observe that those instabilities remain controlled, both in amplitude and frequency. We provide in Table 3 and in Figure 12 information similar to that of Table 1 and Figure 7 for Example 7, illustrating that

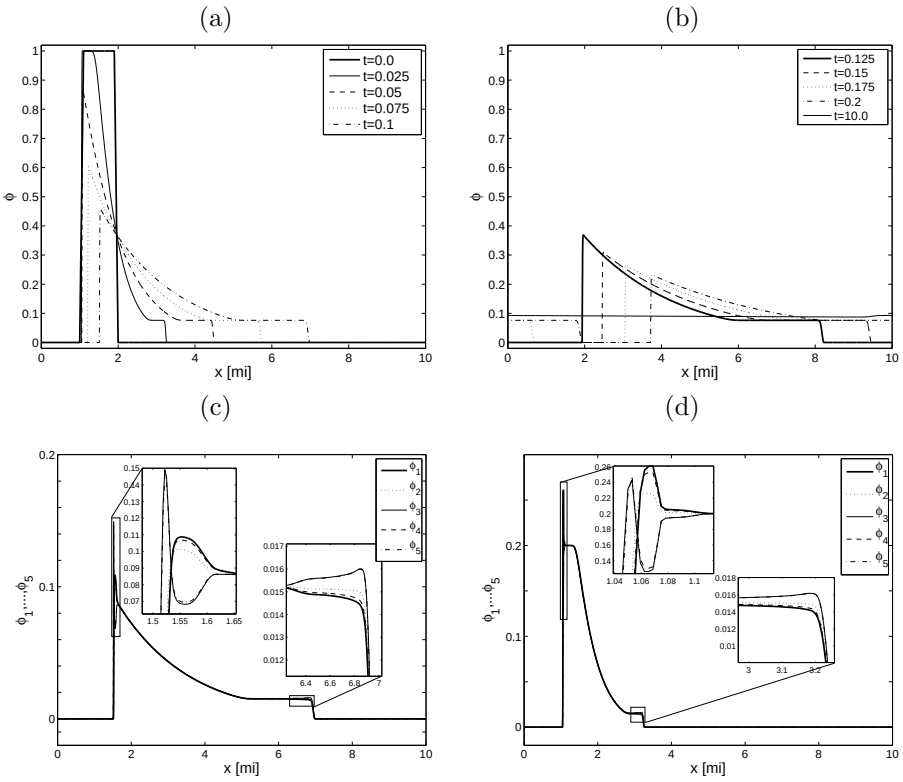

FIGURE 14. Example 12 (DG model, $N = 5$, drivers having the same maximum speed): (a, b) total concentration at different times, (c, d) individual concentrations and enlarged views at times (c) $t = 0.025\,\mathrm{h}$ and (d) $t = 0.1\,\mathrm{h}$.

also for this case, the oscillations observed are not a numerical artifact and that both numerical schemes apparently approximate the same solution.

In Figure 13 we display a time evolution of an initial condition with $\phi_1 = \phi_2 = 0.18$ and a perturbation with amplitude $\delta\phi^0 = 0.05$ in the stability region of B but with some values in the instability region of $\boldsymbol{M}$ (Example 11). We observe that the solution consists of two waves traveling downstream and decreasing in amplitude.

4.5. **Examples 12 and 13 (DG model, $N = 5$, drivers having the same maximum speed).** In Example 12 we consider a circular road of 10 mi and choose $N = 5$ classes of drivers with the same free velocities $v^{\max} = 50\,\mathrm{mi/h}$. To satisfy the parabolicity condition (2.11), it is sufficient to choose reaction times τ_i and anticipation distances L_i such that $\tau_i \le L_i(|\phi V'(\phi)|v^{\max})^{-1}$ for $i = 1, \dots, N$. We employ the DG velocity function (2.5) and choose the reaction times and anticipation distances given in Table 4. Figure 14 shows a time evolution of the initial concentration platoon $\Phi_0(x, 0) = p(x)(0.2, 0.2, 0.2, 0.2, 0.2)^{\mathrm{T}}$, where $p(x)$ is given in (4.2), for which stable behavior is observed.

When condition (2.11) is not satisfied, unstable behavior with non-controlled oscillations appears. As an example (Example 13) we consider the same initial

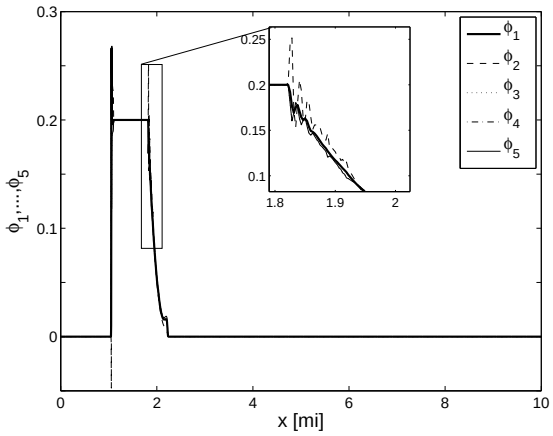

FIGURE 15. Example 13 (DG model, $N = 5$, drivers having the same maximum speed): instabilities may occur when the parabolicity condition (2.11) is not satisfied.

platoon in the previous example but we choose $\tau_2 = 0.00104\,\mathrm{h}$. Simulations are displayed in Figure 15.

5. Conclusions

We have analyzed the stability of a diffusively corrected multiclass Lighthill-Whitham-Richards (DCMCLWR) traffic model that takes into account anticipation lengths and reaction times. The basic result is that to achieve stability, defined in terms of the linearized version (2.8) of (1.6), it is not sufficient to ensure that the diffusion matrix $\boldsymbol{B}$ has eigenvalues with positive real parts; rather, one also has to consider a contribution from the convective part defined by the Jacobian $\boldsymbol{J}$, multiplied by i/ξ. Thus, it is not possible in general to identify stable or unstable solution behaviour with a particular type of (1.6), unless we consider the special cases $\boldsymbol{J} = \boldsymbol{0}$, $\boldsymbol{J}$ being a rank-one perturbation of a multiple of $\boldsymbol{I}$ (as for the case of equal free velocities discussed in Section 2.3) or $\boldsymbol{B} = \boldsymbol{0}$ (as for the standard MCLWR model). This contrasts, for example, with the stability analysis of a model of polydisperse sedimentation [9], whose governing equations can be written as (1.4), and for which a stability analysis similar to the one conducted in Section 2.2 shows that a criterion for stable segregation (formation of horizontal concentration interfaces that move vertically), introduced in [2] for $N = 2$ and supported by experimental results, is equivalent to hyperbolicity of (1.4). The predictions of our linearized stability analysis are confirmed by the numerical experiments in all aspects except that the nonlinearities in the model prevent the amplitude (and in some cases the frequency) of the instabilities to blow up. While we associate oscillations in the numerical solution with unstable behaviour in general, we distinguish between situations where there is a blow-up of frequency (such as in Examples 2, 3, 4 and 13), which means that violations of the stability condition lead to strongly oscillating solutions (akin to those studied in [6]), and situations of mildly unstable behaviour (such as the ones observed in Examples 5 to 8 and 10) with finite frequencies of

oscillation, and where numerical solutions can be interpreted as the formation of stop-and-go waves (although the latter phenomenon is usually associated with much larger amplitudes, cf., e.g., [26, 27]).

Finally, the present model, the stability analysis and its numerical simulations allow us to draw some conclusions of stable and unstable traffic flow caused by heterogeneous drivers' behaviour. To elucidate this issue, let us first point out that the condition (4.3), which is precisely the condition for the scalar equation (1.3) to be (degenerate) parabolic, is very similar to the condition (1.8) derived in [27]. While it is plausible that traffic flow is stable, and for instance free of marked stop-and-go waves, if reaction times of drivers are sufficiently small, our analysis leads to a further conclusion for $N \geq 2$. Namely, for that case it turns out that to ensure stable traffic flow it is not sufficient so require that (4.3) be satisfied with L, τ and $v^{\max}$ replaced by L_i, τ_i and $v_i^{\max}$ for $i = 1, \ldots, N$. This is vividly illustrated in Example 2: two populations of drivers may produce stable traffic flow when separated spatially, however, when they start to "mix", then instabilities occur. This behaviour is essentially produced by the fact that the larger reaction time τ_2 of Species 2 (in Example 2) in not sufficiently small in presence of the significantly faster drivers of class 1. In fact, in view of the assumption (2.1) the criterion (4.1) states that the eigenvalues of $\boldsymbol{B}$ have non-negative real parts (a condition necessary, but in general not sufficient, to ensure stability of traffic flow) if the reaction time τ_i of drivers of a given class i is adapted to the velocities of drivers of the faster classes 1 to $i-1$. In particular, (4.1) means that $\tau_1 \geq \tau_2 \geq \cdots \geq \tau_N$.

Acknowledgments

R. Bürger acknowledges partial support by Fondecyt project 1090456; BASAL project CMM, U. de Chile and Centro de Investigación en Ingeniería Matemática (CI^2MA), Universidad de Concepción; and CONICYT project Anillo ACT1118 (ANANUM). P. Mulet is partially supported by Spanish MCINN MTM2011-22741. L.M.Villada is supported by MECESUP project UCO0713.

References

[1] A. Abeynaike, A.J. Sederman, Y. Khan, M.L. Johns, J.F. Davidson, and M.R. Mackley. The experimental measurement and modelling of sedimentation and creaming for glycerol/biodiesel droplet dispersions. *Chem. Eng. Sci.*, 79:125–137, 2012.

[2] G.K. Batchelor and R.W. Janse van Rensburg. Structure formation in bidisperse sedimentation. *J. Fluid Mech.*, 166:379–407, 1986.

[3] S. Benzoni-Gavage and R.M. Colombo. An n-populations model for traffic flow. *Eur. J. Appl. Math.*, 14:587–612, 2003.

[4] S. Benzoni-Gavage, R.M. Colombo, and P. Gwiazda. Measure valued solutions to conservation laws motivated by traffic modelling. *Proc. Royal Soc. A*, 462:1791–1803, 2006.

[5] S. Berres, R. Bürger, K.H. Karlsen, and E.M. Tory. Strongly degenerate parabolic-hyperbolic systems modeling polydisperse sedimentation with compression. *SIAM J. Appl. Math.*, 64:41–80, 2003.

[6] S. Berres, R. Bürger, and A. Kozakevicius. Numerical approximation of oscillatory solutions of hyperbolic-elliptic systems of conservation laws by multiresolution schemes. *Adv. Appl. Math. Mech.*, 1:581–614, 2009.

[7] R. Bürger, A. García, K.H. Karlsen, and J.D. Towers. A family of numerical schemes for kinematic flows with discontinuous flux. *J. Eng. Math.*, 60:387–425, 2008.

[8] R. Bürger and K.H. Karlsen. On a diffusively corrected kinematic-wave traffic flow model with changing road surface conditions. *Math. Models Methods Appl. Sci.*, 13:1767–1799, 2003.

[9] R. Bürger, K.H. Karlsen, E.M. Tory, and W.L. Wendland. Model equations and instability regions for the sedimentation of polydisperse suspensions of spheres. *ZAMM Z. Angew. Math. Mech.*, 82:699–722, 2002.

[10] R. Bürger, K.H. Karlsen, and J.D. Towers. On some difference schemes and entropy conditions for a class of multi-species kinematic flow models with discontinuous flux. *Netw. Heterog. Media*, 5:461–485, 2010.

[11] R. Bürger and A. Kozakevicius. Adaptive multiresolution WENO schemes for multi-species kinematic flow models. *J. Comput. Phys.*, 224:1190–1222, 2007.

[12] R. Bürger, P. Mulet, and L.M. Villada. Implicit-explicit methods for diffusively corrected multi-species kinematic flow models. Preprint 2012-21, Centro de Investigación en Ingeniería Matemática, Universidad de Concepción; submitted (2012).

[13] A.C. Dick. Speed/flow relationships within an urban area. *Traffic Engrg. Control*, 8:393–396, 1996.

[14] R. Donat and P. Mulet. Characteristic-based schemes for multi-class Lighthill-Whitham-Richards traffic models. *J. Sci. Comput.*, 37:233–250, 2008.

[15] R. Donat and P. Mulet. A secular equation for the Jacobian matrix of certain multi-species kinematic flow models. *Numer. Methods Partial Differential Equations*, 26:159–175, 2010.

[16] H. Greenberg. An analysis of traffic flow. *Oper. Res.*, 7:79–85, 1979.

[17] M. Herty, C. Kirchner, and S. Moutari. Multi-class traffic models on road networks. *Comm. Math. Sci.*, 4:591–608, 2006.

[18] A. Kurganov and A. Polizzi. Non-oscillatory central schemes for traffic flow models with Arrhenius look-ahead dynamics. *Netw. Heterog. Media*, 4:431–451, 2009.

[19] A. Kurganov and E. Tadmor. New high-resolution central schemes for nonlinear conservation laws and convection-diffusion equations. *J. Comput. Phys.*, 160:241–282, 2000.

[20] M.J. Lighthill and G.B. Whitham. On kinematic waves: II. A theory of traffic flow on long crowded roads. *Proc. Royal Soc. A*, 229:317–345, 1955.

[21] S. Logghe and L.H. Immers. Multi-class kinematic wave theory of traffic flow. *Transp. Res. B*, 42:523–541, 2008.

[22] P. Nelson. Synchronized traffic flow from a modified Lighthill-Whitman model. *Phys. Rev. E*, 61:R6062–R6055, 2000.

[23] P. Nelson. Traveling-wave solution of the diffusively corrected kinematic-wave model. *Math. Comp. Modelling*, 35:561–579, 2002.

[24] D. Ngoduy. Multiclass first-order modelling of traffic networks using discontinuous flow-density relationships. *Transportmetrica*, 6:121–141, 2010.

[25] D. Ngoduy. Multiclass first-order traffic model using stochastic fundamental diagrams. *Transportmetrica*, 7:111–125, 2011.

[26] D. Ngoduy. Effect of driver behaviours on the formation and dissipation of traffic flow instabilities. *Nonlin. Dynamics*, 69:969–975, 2012.

[27] D. Ngoduy and C. Tampere. Macroscopic effect of reaction time on traffic flow characteristics. *Physica Scripta*, 80:paper 025802, 2009.

[28] P.I. Richards. Shock waves on the highway. *Oper. Res.*, 4:42–51, 1956.

[29] E. Rouvre and G. Gagneux. Solution forte entropique de lois scalaires hyperboliques-paraboliques dégénérées. *C. R. Acad. Sci. Paris Sér. I*, 329:599–602, 1999.

[30] F. Siebel and W. Mauser. On the fundamental diagram of traffic flow. *SIAM J. Appl. Math.*, 66:1150–1162, 2006.

[31] A. Sopasakis and M.A. Katsoulakis. Stochastic modeling and simulation of traffic flow: asymmetric single exclusion process with Arrhenius look-ahead dynamics. *SIAM J. Appl. Math.*, 66:921–944, 2006.

[32] M. Treiber, A. Kesting, and D. Helbing. Influence of reaction times and anticipation on stability of vehicular traffic flow. *Transp. Res. Record* no. 1999, 23–29, 2007.

[33] G.C.K. Wong and S.C. Wong. A multi-class traffic flow model—an extension of LWR model with heterogeneous drivers. *Transp. Res. A*, 36:827–841, 2002.

[34] M. Zhang, C.-W. Shu, G.C.K. Wong, and S.C. Wong. A weighted essentially non-oscillatory numerical scheme for a multi-class Lighthill-Whitham-Richards traffic flow model. *J. Comput. Phys.*, 191:639–659, 2003.

[35] P. Zhang, R.-X. Liu, S.C. Wong, and S.Q. Dai. Hyperbolicity and kinematic waves of a class of multi-population partial differential equations. *Eur. J. Appl. Math.*, 17:171–200, 2006.

[36] P. Zhang, S.C. Wong, and S.-Q. Dai. A note on the weighted essentially non-oscillatory numerical scheme for a multi-class Lighthill-Whitham-Richards traffic flow model. *Comm. Numer. Meth. Engrg.*, 25:1120–1126, 2009.

[37] P. Zhang, S.C. Wong, and C.-W. Shu. A weighted essentially non-oscillatory numerical scheme for a multi-class traffic flow model on an inhomogeneous highway. *J. Comput. Phys.*, 212:739–756, 2006.

[38] P. Zhang, S.C. Wong, and Z. Xu. A hybrid scheme for solving a multi-class traffic flow model with complex wave breaking. *Comput. Meth. Appl. Mech. Engrg.*, 197:3816–3827, 2008.

Centro de Investigación en Ingeniería Matemática (CI^{2}MA)

PRE-PUBLICACIONES 2012

2012-14 Emilio Cariaga, Rubén Martínez, Mauricio Sepúlveda: *Estimation of hydraulic parameters under unsaturated flow conditions in heap leaching*

2012-15 Rodolfo Araya, Christopher Harder, Diego Paredes, Frederic Valentin: *Multiscale hybrid-mixed method*

2012-16 Alfredo Bermúdez, Bibiana López-Rodríguez, Rodolfo Rodríguez, Pilar Salgado: *An eddy current problem in terms of a time-primitive of the electric field with non-local source conditions*

2012-17 Gabriel N. Gatica, Antonio Marquez, Walter Rudolph: *A priori and a posteriori error analyses of augmented twofold saddle point formulations for nonlinear elasticity problems*

2012-18 Raimund Bürger, Enrique D. Fernández Nieto, El Hadji Koné, Tomás Morales De Luna: *A multilayer shallow water system for polydisperse sedimentation*

2012-19 Fabián Flores-Bazán, Giandomenico Mastroeni: *Strong duality in cone constrained nonconvex optimization: a general approach with applications to nonconvex variational problems*

2012-20 Alfredo Bermúdez, Dolores Gómez, Rodolfo Rodríguez, Pilar Salgado, Pablo Venegas: *Numerical solution of a transient non-linear axisymmetric eddy current model with non-local boundary conditions*

2012-21 Raimund Bürger, Pep Mulet, Luis M. Villada: *Implicit-explicit methods for diffusively corrected multi-species kinematic flow models*

2012-22 Raimund Bürger, Stefan Diehl: *Convexity-preserving flux identification for scalar conservation laws modelling sedimentation*

2012-23 Raimund Bürger, Ilja Kröker, Christian Rohde: *A hybrid stochastic Galerkin method for uncertainty quantification applied to a conservation law modelling a clarifier-thickener unit*

2012-24 Felipe Lepe, David Mora, Rodolfo Rodríguez: *Locking-free finite element method for a bending moment formulation of Timoshenko beams*

2012-25 Raimund Bürger, Pep Mulet, Luis M. Villada: *A diffusively corrected multi-class Lighthill-Whitham-Richards traffic model with anticipation lengths and reaction times*

Para obtener copias de las Pre-Publicaciones, escribir o llamar a: Director, Centro de Investigación en Ingeniería Matemática, Universidad de Concepción, Casilla 160-C, Concepción, Chile, Tel.: 41-2661324, o bien, visitar la página web del centro: `http://www.ci2ma.udec.cl`







Centro de Investigación en
Ingeniería Matemática (CI²MA)
Universidad de Concepción

Casilla 160-C, Concepción, Chile
Tel.: 56-41-2661324/2661554/2661316
http://www.ci2ma.udec.cl